Design of an Expanding Cosmological Background for the Moving Punctures approach to Numerical Relativity

Bachelor Thesis

Grau en Enginyeria Física - Grau en Matemàtiques

Author: Jordi Manyer Fuertes

Supervisor: Deirdre Shoemaker, Dunn Family Professor of Physics

Co-Supervisor: Pablo Laguna, School of Physics chair and Professor

Tutor: Narciso Román-Roy, Professor

Center for Relativistic Astrophysics

School of physics, Georgia Institute of Technology

Barcelona School of Telecommunications Engineering (ETSETB)

Universitat Politècnica de Catalunya

Barcelona School of Mathematics and Statistics (FME)

Universitat Politècnica de Catalunya

Centre de Formació Interdisciplinària Superior (CFIS)

Universitat Politècnica de Catalunya

May 17, 2019

Acknowledgements

I would like to thank Prof. Deirdre Shoemaker for the great opportunity she has given me to work in her research group at Georgia Tech, doing research in one of the most exiting fields theoretical physics has to offer.
I would also like to thank Prof. Pablo Laguna for putting together and supervising this project, for solving my doubts and being my theoretical backbone. I hope this project continues prospering and I look forward to reaching the point where it can be published.
Finally I would like to thank Prof. Narciso Román-Roy for being my supervisor in Barcelona, to the CFIS program for the economical support and to Prof. Tamara Bogdanović for being the original contact that made this opportunity possible.

Thanks to all the members of the Numerical Relativity team, you have been great friends and co-workers. Special thanks to Bhavesh and Miguel for their help throughout the project.
Thanks to my international family, and thanks to Scott who made it possible. To Chiara, Joan, Irene and Pietro: Our friendship is one of the most precious things I bring back from Atlanta.
Thanks to my friends in Barcelona for being as amazing as they always are.

Finally to my family, who has always been there, and to Marina, who hopefully always will. This is because of you.

Abstract

Predicted in 1916 by Albert Einstein in his theory of general relativity, gravitational waves are now at the heart of modern astrophysics. Created in some of the most energetic events in the universe, such as binary black hole collisions, neutron star collisions or the big bang, this ripples of space time offer a completely new spectrum for the study of the universe, possibly allowing scientists to get an insight on previously unseen phenomena.

In this context, numerical relativity becomes important as a tool to simulate these high-energy systems and calculate the resulting gravitational waves. As we wait for the new generation of laser interferometers, the field has to find ways to keep up with the increasing demand in accuracy. It is therefore important to study and tackle all the possible sources of error that the simulations might have.
One of the simplifications numeral relativity codes usually do is to consider the supermassive bodies isolated in an otherwise massless non-expanding universe (a Minkowski background). Although it is a fairly good approximation, it is still physically inaccurate and a potential source of error.

This work aims to start exploring the possibility of new cosmological backgrounds for black hole simulations. Specifically, we consider a particular metric, the Friedmann-Lemaître-Robertson-Walker cosmology, and provide a full guided development on how to adapt a state-of-the-art numerical relativity code, the Einstein Toolkit, to use that metric as a background for black hole simulations. We then proceed to show results from simulations we performed using that specific theoretical development.

Keywords— Numerical Relativity, Gravitational Waves, Einstein Field Equations, FLRW metric, Friedmann-Lemaître-Robertson-Walker metric, Expanding Cosmology , Physics, General Relativity, Numerical Calculus, Black Hole, Black Hole Binaries

Contents

List of Figures

1 Introduction

Predicted in 1916 by Albert Einstein in his theory of general relativity, gravitational waves are now at the heart of modern astrophysics. Created in some of the most energetic events in the universe, such as binary black hole collisions, neutron star collisions or the big bang, this ripples of space time offer a completely new spectrum for the study of the universe, possibly allowing scientists to get an insight on previously unseen phenomena [12, 13]. Their non-matter-interactive nature allows them to carry unaltered information from the edges of the universe, making them essential to explore places where electromagnetic waves and particles cannot travel.

Gravitational waves were first observed in 1974, when Russell Alan Hulse and Joseph Hooton Taylor discovered a pulsar-star binary system (later known as the Hustle-Taylor binary). By measuring the change in the period of the binary's orbit over almost a decade, they determined that that change was produced by the radiation of gravitational waves (and the consequent loss of energy), indirectly detecting gravitational waves for the first time, earning them the physics Nobel prize in 1993.
The first direct observation of gravitational waves came on September 14, 2015, as a result of the Laser Interferometer Gravitational-Wave Observatory (LIGO) project [37, 49]. This event, GW150914, represented a milestone for the field of astrophysics and a hole new realm of possibilities to explore. Since then, LIGO has provided more than 10 detections and it is still improving. It is expected to get to design sensitivity in 2020. Moreover, the Laser Interferometer Space Antenna (LISA) project [19], the space-based counterpart of the ground-based detector LIGO, is supposed to start collecting data in less than 20 years. Both of this future events will provide a very substantial increase in sensitivity, allowing scientists to observe events that are further away and/or less energetic.
Other interferometers, such as Virgo [14] and GEO [51], will also be improving and providing more accurate detections of gravitational waves.

The theory of general relativity predicts that gravitational waves should serve essentially as a physical fingerprint for each gravitational event, allowing us to deduce the fundamental parameters of the original system from the detections [11]. But the theory of General Relativity , as beautifully simple and elegant as it may seem, is a very complex system of ten coupled and non-linear four-dimensional partial differential equations. Therefore it can only be solved for very specific and highly symmetric systems. Black hole and star binaries are not among those, thus numerical integration techniques are needed to model the systems, evolve them in time and finally obtain the desired gravitational waves.
In order to process the raw data provided by LIGO, find gravitational wave events inside the live stream of data and be able to separate noise from actual detections, a gravitational wave template bank has to be created. This catalogue should cover a wide enough range of initial parameters so that every LIGO-detectable event could be found by searching for correlations between the raw data and the templates in the catalogue of waves.

This catalogue is being created by a handful of research groups [41, 44, 56, 70], but the predicted increase in sensibility that will be provided in the near future by both design-sensibility LIGO and LISA are pushing the need for more accurate simulations and a wider parameter space. With that objective in mind, new methods need to be developed.

One of the simplifications numeral relativity codes usually do is to consider the supermassive bodies isolated in an otherwise massless non-expanding universe (a Minkowski background). Although it is a fairly good approximation, it is still physically inaccurate and a potential source of error.
This work aims to start exploring the possibility of new cosmological backgrounds for black hole simulations. Specifically, we consider a particular metric, the Friedmann-Lemaître-Robertson-Walker cosmology, and provide a full guided development on how to adapt a state-of-the-art numerical relativity code, the Einstein Toolkit, to use that metric as a background for black hole simulations. We then proceed to show results from simulations we performed using that specific theoretical development.

This essay will be structured in the following way: We will first have a look the state of numerical relativity today from a theoretical point of view, i.e how the Einstein equations are transformed into a Cauchy problem and all the difficulties that arise when doing it. We will then introduce the Cactus Framework and the Einstein Toolkit, the open-source state-of-the-art code that we have used to produce our simulations. Finally, we will present our work, both theoretical and practical aspects, as explained in the previous paragraph.

2 Theoretical background

The aim of this section is to set the basis of numerical relativity, starting from the 3+1 foliation of space-time, the projection of Einstein equations into this decomposed geometry to obtain the ADM equations and the further modification of this equations to obtain the BSSNOK formulation that is currently in use. We will also discuss the choice of gauge equations, as this notion will be important for later sections.
We will not discuss however the mathematical background necessary to follow this chapter, including very important differential geometry concepts as Lie and Covariant derivatives, Christoffel symbols, etc... For a formal numerical relativity-oriented overview of this mathematical background please refer to [39].
Neither will we discuss in detail basic concepts of General Relativity such as the Einstein field equations.

2.1 Geometrized Unit system

Throughout this work, and most naturally for general relativity, we will take as standard the **Geometrized Unit System** [54]. This system consists in taking

$$c = G = k_B = 1 \tag{1}$$

where c is the speed of light, G is Newton's gravitational constant and k_B is Boltzman's constant. A full conversion table can be found in [54].

This system is practical for two main reasons:
The obvious reason is that in general relativity those constants appear in almost every equation, and therefore setting them to unity allows for a more elegant theoretical development of the physics.
What is a little more subtle but arguably more important is that this systems makes both mass, length and time have units of length. This is important because it will make our simulations "scalable" and reduce our parameter space. In short, the metric for a non-spinning black hole in vacuum (a Swartzschild metric) will not depend on how big the black hole is (on his mass). We will always set the total mass of our system to unity, and then the results can be scaled accordingly with each particular mass and all quantities (time, space, ...) will scale with it. I.e. by evolving a single space-time we will get the solution for all the equivalent systems no matter the mass.
In fact, most of the literature gives both time and space measures in units of $\mathcal{M}$, which is nothing more than the total mass of the system.

2.2 3+1 Decomposition and ADM equations

Probably one of the most elegant features of general relativity is the fact that it unifies space and time into a single 4-dimensional space-time where all four dimensions are treated equally. This

is not very practical however when numerically implementing these equations, and it is therefore imperative to decouple one of the dimensions from the other three so that numerical integration is possible. This process is called 3+1 decomposition and vastly dominates the literature, thus there are plenty of texts that develop it. We will be following [73], [15], [25] and [39].
Although in theory any of the four dimensions could be separated from the others, historically one distinguishes time over the three spatial dimensions, making for the most intuitive and easily treatable approach possible. Space-time is therefore sliced into a set of fully space-like hypersurfaces embedded into the 4-dimensional space-time (see Figure 1[1]).
It needs to be noted that not every space-time can be sliced in this manner: The ones that can are called "globally hyperbolic", and are characterised by not having closed time-like curves (they don't allow time travel to the past). We will from now on assume that all the space-times considered fulfil this condition, which is true for most of the space-times of interest.

2.2.1 The lapse function

Given one of this foliations $\{\Sigma_t\}_{t\geq 0}$, we can parameterise it with a parameter t such that every hypersurface is defined as a level surface of t. Given a hypersurface Σ_t, the gradient 1-from $\boldsymbol{dt}$ and it's metric dual vector $\vec{\boldsymbol{\nabla}}t$ are both normal to Σ_t. We can then define an unitary normal vector $\mathbf{n}$ as

$$\boldsymbol{n} = \pm(\vec{\boldsymbol{\nabla}}t \cdot \vec{\boldsymbol{\nabla}}t)^{-1/2}\vec{\boldsymbol{\nabla}}t \quad \text{such that} \boldsymbol{n}\cdot\boldsymbol{n} = -1$$

It can be shown that both $\vec{\boldsymbol{\nabla}}t$ and $\boldsymbol{n}$ are in fact time-like. They are of course collinear by construction and we can write

$$\boldsymbol{n} = \alpha\vec{\boldsymbol{\nabla}}t \quad \text{with} \quad \alpha = \pm(\vec{\boldsymbol{\nabla}}t \cdot \vec{\boldsymbol{\nabla}}t)^{-1/2}$$

α is called the **lapse function**, and can be shown to be the rate between the proper time τ of an Eulerian observer (defined as an observer with 4-velocity equal to $\boldsymbol{n}$) and the time coordinate t:

$$d\tau = \alpha\ dt \tag{2}$$

2.2.2 The shift vector

Given a particular coordinate system for the foliation, we can also define $\boldsymbol{\partial}_\alpha = (\boldsymbol{\partial}_t, \boldsymbol{\partial}_i)$ as the natural vector basis in the 4-dimensional space-time associated with the coordinates (x^α), such that

$$\boldsymbol{\partial}_t := \frac{\partial}{\partial t} \qquad \boldsymbol{\partial}_i := \frac{\partial}{\partial x^i}$$

It can be shown that $\boldsymbol{\partial}_t$ is tangent to the lines of constant spatial coordinates and that $\boldsymbol{\partial}_i$ define a base for Σ_t's tangent space $T_p(\Sigma_t)$. $\boldsymbol{\partial}_t$ is called the time vector, and generally differs from $\boldsymbol{n}$. It can be shown that

[1] Figure taken and modified from [39]

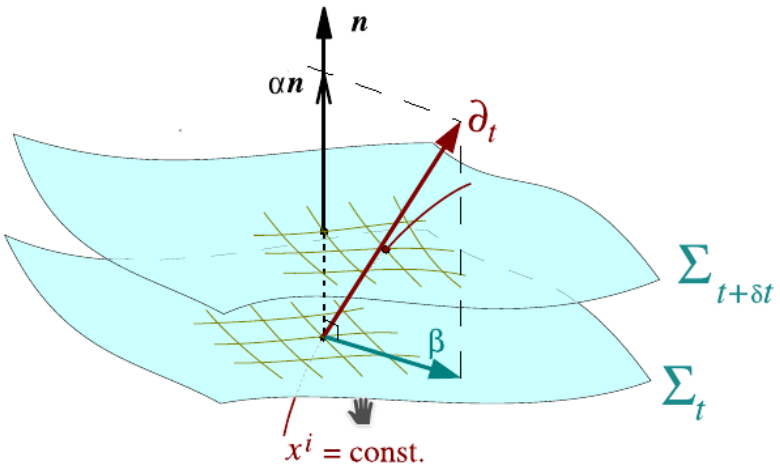

Figure 1: Foliation of Space-time into space-like hypersurfaces.

$$\langle \boldsymbol{d}t, \boldsymbol{\partial} t \rangle = \langle \boldsymbol{d}t, \alpha \boldsymbol{n} \rangle = 1$$

This property allows us to uniquely choose a space-like vector (tangent to Σ_t) $\boldsymbol{\beta} = \beta^i \boldsymbol{\partial}_i$ such that

$$\boldsymbol{\partial}_t = \alpha \boldsymbol{n} + \boldsymbol{\beta} \tag{3}$$

Because $\boldsymbol{n}$ is time-like and $\boldsymbol{\beta}$ is space-like, this is actually a 3+1 decomposition of $\boldsymbol{\delta}_t$.
$\boldsymbol{\beta}$ is called the **Shift vector** and represents the relative velocity between the Eulerian observers and the lines of constant spacial coordinates.
It must also be noted that the normal vector $\boldsymbol{n}$ can be written in terms of α and $\boldsymbol{\beta}$ and the coordinates using equation (3):

$$n^\mu = (1/\alpha, -\beta^i/\alpha) \tag{4}$$

2.2.3 Decomposition of the metric and choice of coordinates

As we have seen, given a space-time $g_{\mu\nu}$, a space-like foliation $\{\Sigma_t\}$ and a set of coordinates (x^α), we can uniquely determine a scalar field $\alpha = \alpha(t, x^i)$ and a space-like vector field $\boldsymbol{\beta} = \boldsymbol{\beta}(t, x^i)$.
The converse is also locally true in the sense that given a starting hypersurface Σ_0 with **local metric** γ_{ij} and fields α and $\boldsymbol{\beta}$, both the 4-dimensional metric $g_{\mu\nu}$ and the foliation $\{\Sigma_t\}$ can be uniquely determined:
The metric will be given by

$$ds^2 = (-\alpha^2 + \beta_i \beta^i) dt^2 + 2\alpha\beta_i dx^i + \gamma_{ij} dx^i dx^j \tag{5}$$

and the "next" hypersurface of the foliation $\Sigma_{\delta t}$ will be constructed by Lie transporting Σ_0 along the vector $\alpha \boldsymbol{n}$.

This means that a choice for $\{\alpha, \boldsymbol{\beta}, \gamma_{ij}\}$ is effectively a choice for our space-time metric, our foliation of this space-time and a coordinate system on each hypersurface of the foliation.

This approach will be the one used in the numerical relativity codes to set up and evolve initial conditions.
The choice for α and β is of course not unique as we can reparametrize the coordinate system to obtain the same overall 4-dimensional metric. This means α and β offer a choice of coordinates, that is extremely important in numerical relativity. They are called **Gauge Variables** and we will discuss the importance of their choice in sec.2.5.
Given $\{\alpha, \boldsymbol{\beta}, \gamma_{ij}\}$, the explicit forms for the four-dimensional metric and the normal vector are:

$$g_{\mu\nu} = \begin{pmatrix} -\alpha^2 + \beta_k\beta^k & \beta_i \\ \beta_j & \gamma_{ij} \end{pmatrix} \tag{6}$$

$$g^{\mu\nu} = \begin{pmatrix} -1/\alpha^2 & \beta^i/\alpha^2 \\ \beta^j/\alpha^2 & \gamma^{ij} - \beta^i\beta^j/\alpha^2 \end{pmatrix} \tag{7}$$

$$n^\mu = \left(1/\alpha, -\beta^i/\alpha\right), \quad n_\mu = (-\alpha, 0), \quad n^\mu n_\mu = -1 \tag{8}$$

Is is also important to note that because of this decomposition of the metric we will introduce some notation mechanics that will make work easier:

- Four-dimensional tensors will have Greek indexing ($G_{\mu\nu}$, etc...) and the manipulation of indexes will be done using the four-dimensional metric $g_{\alpha\beta}$.
- Three-dimensional tensors will have Latin indexing (β^i, etc...) and the manipulation of indexes will be done using the three-dimensional metric γ_{ij}.

We will assume this mechanics and will not be explicit about them from now on.

2.2.4 Projection operators and Extrinsic Curvature

In order to go from the raw Einstein equations to their 3+1 from, we will need to disentangle time from space by projecting them into the normal and spatial components. To do that, we will define our projection operator

$$P^\mu_\nu := \delta^\mu_\nu + n^\mu n_\nu \tag{9}$$

Defined this way, P^μ_ν is the projection operator into tangent space of the hypersurface Σ_t. Keeping in mind that $n^\mu n_\mu = -1$, it is easy to see that, for any vector v^ν,

$$(P^\mu_\nu v^\nu) n_\mu = 0 \ , \tag{10}$$

i.e that the normal component of the projected vector is null, which proves that P^μ_ν indeed projects any vector into $T_p(\Sigma_t)$ since normal and tangent spaces are orthogonal complements.
This operator can also be easily extended to project arbitrary-order tensors by simply contracting all free indices one at a time. For instance, we define for two-covariant tensors

$$PT_{\mu\nu} := P^\epsilon_\mu P^\rho_\nu T_{\epsilon\rho} \ . \tag{11}$$

Using the projection operator, we can also define the **Extrinsic Curvature tensor** as follows:

$$K_{\mu\nu} := -P(\boldsymbol{\nabla}_\mu n_\nu) = -\nabla_\mu n_\nu - n_\mu n^\epsilon \nabla_\epsilon n_\nu \ . \tag{12}$$

where ∇_μ is the covariant derivative that can be written using Christoffel symbols as

$$\nabla_\mu n_\nu = \partial_\mu n_\nu - \Gamma^\epsilon_{\mu\nu} n_\epsilon \ . \tag{13}$$

$K_{\mu\nu}$ can be shown to be both symmetric and purely spatial, and for that reason we will only consider it's spatial components K_{ij}.

This tensor will be extremely important for the ADM formulation, and must not be confused with the **Intrinsic Curvature tensor** R_{ij} which is nothing more that the three-dimensional Riemann tensor defined in terms of γ_{ij}. The intrinsic curvature is defined purely with the three-dimensional metric and therefore is intrinsic to the metric in the sense that it does not depend on how the surface is embedded in the four-dimensional space-time.
The extrinsic curvature, on the other hand, reveals how the surface curves into the four-dimensional space-time. A very intuitive way of looking at it is to look at how it has been defined: If $\boldsymbol{n}$ is the normal vector field, defined in every point of the surface, $\nabla_\mu n_\nu$ quantifies the change of the normal vector when we move over the surface, which in turn is equivalent to quantify how the surface bends in the four-dimensional space-time. $K_{\mu\nu}$ is not other than the spacial projection of this quantity.
It must be noted that this way of defining the extrinsic curvature is highly simplistic and can appear as arbitrary. This is not the case, as this definition derives from a more formal approach that can be found in [39] and that involves the Weingarten map and the Second Fundamental Form of the surface.

By operating on (12) one can show that

$$K_{ij} := \frac{1}{2\alpha}\left(-\partial_t \gamma_{ij} + D_i\beta_j + D_j\beta_i\right) \tag{14}$$

and from (14) we deduce that

$$\partial_t \gamma_{ij} = -2\alpha K_{ij} + D_i\beta_j + D_j\beta_i \tag{15}$$

Using the concept of Lie derivative, equation (15) can be rewritten as

$$\left(\partial_t - \pounds_{\boldsymbol{\beta}}\right)\gamma_{ij} = \pounds_{\alpha\boldsymbol{n}}\gamma_{ij} = -2\alpha K_{ij} \tag{16}$$

The process can be found in [15]. Although equation (16) is more elegant, the evolution of the metric will be coded using (15). With this equation, we only need an equation for the evolution of K_{ij} complete the evolution system. That equation will come from the Einstein field equations.

2.2.5 ADM equations

The rest of the equations we need to close the system will come from the Einstein field equations

$$G_{\mu\nu} = 8\pi T_{\mu\nu} \tag{17}$$

where $T_{\mu\nu}$ is the Stress-Energy tensor (holding all the mass and energy information) and $G_{\mu\nu}$ is the Einstein tensor (holding all the geometric information). $T_{\mu\nu}$ depends on the configuration of matter and energy, and will be further developed in sec.2.6 and $G_{\mu\nu}$ is defined as

$$G_{\mu\nu} = R_{\mu\nu} - \frac{1}{2} g_{\mu\nu} R \ . \tag{18}$$

Here $R_{\mu\nu}$ and R are respectively the four-dimensional Ricci tensor and scalar (both depend exclusively on the four-dimensional metric).

By projecting this equations using the normal vector and the projection operator, we can divide them in three groups:

- Fully temporal projection

$$n^\mu n^\nu \left(G_{\mu\nu} - 8\pi T_{\mu\nu}\right) = 0 \tag{19}$$

- Mixed projections

$$P n^\mu \left(G_{\mu\nu} - 8\pi T_{\mu\nu}\right) = 0 \tag{20}$$

- Fully spatial projections

$$P \left(G_{\mu\nu} - 8\pi T_{\mu\nu}\right) = 0 \tag{21}$$

This three expressions are then developed to obtain the final equations. The development can be interesting as it uses the Gauss,Ricci and Codazzi equations, but it is also long and can be found in numerous text so we will take the freedom of not reproducing it here. To whoever can be interested, refer to [39] for the full development. We will simply give the resulting equations here:

- From the fully temporal projection (19), we get

$$R^{(3)} + K^2 - K_{ij} K^{ij} = 16\pi u \tag{22}$$

  where $R^{(3)}$ is the Riemann scalar derived from the three-dimensional Riemann tensor, K is the trace of the extrinsic curvature and u is the energy density as measured by Eulerian observers, defined as

$$u := n_\mu n_\nu T^{\mu\nu} \tag{23}$$

- From the mixed projections (20), we get

$$D_j \left[K^{ij} - \gamma^{ij} K\right] = 8\pi j^i \tag{24}$$

with $\boldsymbol{j}$ is the momentum flux of matter as measured by Eulerian observers and defined as

$$j^i := P^i_\mu \left(n_\nu T^{\mu\nu}\right) \tag{25}$$

- From the fully spatial projections (21) we get

$$\begin{aligned} \partial_t K_{ij} = {} & \beta^k \partial_k K_{ij} + K_{ik}\partial_j \beta^k + K_{jk}\partial_i \beta^k \\ & - D_i D_j \alpha + \alpha \left[R^{(3)}_{ij} - 2K_{ik}K^k_j + K K_{ij}\right] \\ & + 4\pi\alpha \left[\gamma_{ij}(S-u) - 2S_{ij}\right] \end{aligned} \tag{26}$$

where S_{ij} is the stress tensor of matter defined as

$$S_{ij} = P T_{ij} \tag{27}$$

and S is it's trace.
Like for eq.(15), (26) can be rewritten using the Lie derivative and takes the form

$$\begin{aligned} \pounds_{\alpha \boldsymbol{n}} K_{ij} = {} & -D_i D_j \alpha + \alpha \left[R^{(3)}_{ij} - 2K_{ik}K^k_j + K K_{ij}\right] \\ & + 4\pi\alpha \left[\gamma_{ij}(S-u) - 2S_{ij}\right] \ . \end{aligned} \tag{28}$$

First, we should note that (22) and (24) are a set of four equations that do not have any temporal derivatives. Indeed they are not evolution equations for our system and are instead called constraints as they should be fulfilled by the system at any given time. Eq.(22) and eqs.(24) are called respectively Hamiltonian (or Energy) and Momentum constraints, and show that not every arbitrary combination of values for $\{\gamma_{ij}, K_{ij}, T_{\mu\nu}\}$ is a possible Einstein space.
The six remaining equations (26) contain the missing dynamics of our system and coupled with eqs.(15) they form a closes system of evolution equations for the geometric variables of the system. They are know as Arnowitt-Deser-Misner (ADM) equations and must be paired with evolution equations for $T_{\mu\nu}$ (that will be discussed in sec.2.6). Although the equations bear Arnowitt, Deser and Misner's name for their work in 1962 [22], the current state of the equations was adopted later in [82]. The original equations in [22] used the momentum conjugate to the metric π_{ij} instead of the extrinsic curvature.

It is also worth noting that, although the Hamiltonian and Momentum constraints should in theory be calculated at every step to confirm that they hold, by using the Bianchi identities we can actually prove that the evolution equations preserve the constraints, i.e that if the constraints hold for a system $\{\gamma_{ij}, K_{ij}, T_{\mu\nu}\}$ they will automatically hold for that same system at any point in time provided it has been evolved using the ADM equations.

In practice, we will solve the constraints to find the initial conditions of our system (which is not easy as we will see in sec.2.4) and then calculate them at every iteration (not solve them!) as an indicator of how accurate our evolved system is.

2.3 Conformal decomposition and BSSNOK formulation

Although the ADM equations (16) and (28) are enough to evolve our system, the Cauchy problem needs initial data to evolve from. This is not a trivial problem as will be discussed by section 2.4 and demands a very important change of variables in the evolution equations.
This process will be called **conformal decomposition** and was introduced in 1944 by Lichnerowicz [48] as a tool for solving the initial data problem. Then, in the 1970's York [77, 79] showed that conformal decompositions are also important for the time evolution problem. It is now know to be crutial for the numerical implementation of the solutions, as we will explain in section 2.3.1.
Although we will not go into mathematical detail, we will try to expose the most significant aspects of the conformal tranformations like the notion of hyperbolicity. We will also give the original conformal evolution equations, as well as further developments made by Shimata and Nakamura in 1995 [67] and by Baumgarte and Shapiro in 1999 [24] to obtain the Baumgarte-Shapiro-Shibata-Nakamura (BSSN) evolution scheme that we use in our simulations. A full mathematical development of this section can be found in [39].

2.3.1 Hyperbolicity of the evolution equations

Hyperbolicity is a concept general to all PDE systems concerning existence and stability of solutions, but that plays an important role in numerical relativity as we will explain in this section. A more detailed description of the concept of hyperbolicity can be found in [45].
Consider a one-dimensional (the concept can be generalised to higher dimensions), first-order (any system can be made first-order by adding variables) and linear system of PDEs

$$\partial_t u_i = \sum_j M_{ij} \partial_x u_j = q_i \qquad i \in \{1, ..., n\} \ , \tag{29}$$

or in matrix form

$$\boldsymbol{u} + M \partial_x \boldsymbol{u} = \boldsymbol{q} \ . \tag{30}$$

The system is said to be **hyperbolic** if all of M's eigenvalues are real functions, and **strongly hyperbolic** if there also exist a complete set of eigenvectors (if not, the system is called **weakly hyperbolic**).
In a physical sense, hyperbolicity implies that the system is causal and local. It can also be mathematically proven that a strongly hyperbolic system is well posed in the sense that given a set of initial conditions the solution of the system exists, is unique, and that small perturbations in the initial data result only in small changes in the solution.

As we have mentioned before, the ADM equations 16 and 28 as given here are not in the

original form given by Arnowitt, Deser and Misner in [22] but rather in a revisited form given by York in [82].
Although the most visible change is the replacement of the canonical conjugate momentum π_{ij} by the extrinsic curvature K_{ij}, there is another minor but important change to the equations: If we rewrite the original ADM equations with the extrinsic curvature, we would obtain an equation for K_{ij} that differs from ours (28) by a multiple of the Hamiltonian constraint.
Indeed, the fact that the system has constraints (basically expressions of our variables that amount to zero) implies a non-unicity of the evolution equations. We can always add or subtract any multiple of the constraints to obtain another evolution scheme that has the same solutions than the original one **as long as the constraints hold**. However, the complete set of solutions is not the same for both sets of evolution equations: The solutions only coincide in a subset of solutions, called the **constraint hypersurface**, where the constraints hold (i.e. the set of solutions with physical meaning).

If we were solving the system analytically, both sets of equations would therefore be equivalent. As this is impossible for the majority of systems of interest, we are forced to consider how numerical error will affect our equations. In particular, we are bound to ask ourselves how small violations of the constraints (inevitable in numerical simulations) might affect the final solution. In other words, how different is a solution that is slightly not in the constraint hypersurface to another that is.
Since the constraints have second derivatives of the metric, adding or subtracting multiples of those constraints affects greatly the structure of the differential equations, changing the system from hyperbolic to elliptic, or even from well-posed to ill-posed. It is then important to consider the way the evolution equations are written. Which is the best way to write them is still an open problem, but throughout this section we will try to give a taste on how this problem has been treated so far.

2.3.2 Conformal Decomposition

The conformal decomposition as presented by Lichnerowicz and York [48, 77, 79] is at core a transformation in the spatial metric of the form:

$$\gamma_{ij} = \psi^4 \tilde{\gamma}_{ij} \tag{31}$$

where $\tilde{\gamma}_{ij}$ is called the **conformal metric** and is considered known. The transformation is said to be conformal because it can be shown to preserve angles.
In addition to this change, the extrinsic curvature is also split into it's trace and it's traceless part:

$$K_{ij} \quad \longrightarrow \quad \begin{cases} K = \gamma^{ij} K_{ij} \\ A_{ij} := K_{ij} - \frac{1}{3}\gamma_{ij} K \end{cases} \tag{32}$$

We will also develop a conformal transformation for the **traceless extrinsic curvature** A_{ij}. In fact, two versions of this transformation are present in the literature:

$$\tilde{A_{ij}} = \psi^{-4} A_{ij} \tag{33}$$

$$\hat{A_{ij}} = \psi^{-10} A_{ij} \ . \tag{34}$$

Both transformations are useful and will be used for different purposes: $\tilde{A_{ij}}$ is used while considering the conformal transformation of the evolution equations, while $\hat{A_{ij}}$ is used for computing initial data for black hole binaries as we will see in sec.2.4.

The original conformal transformation chooses

$$\psi = \left(\frac{\gamma}{f}\right)^{1/12} \tag{35}$$

where f_{ij} is a **background metric** and

$$\gamma = det(\gamma_{ij}) \quad \text{and} \quad f = det(f_{ij}) \ . \tag{36}$$

A background metric is a metric chosen such that it is Riemannian like γ_{ij} (with full positive signature) and such that

$$\frac{\partial f_{ij}}{\partial t} = 0 \ . \tag{37}$$

This definition of the background metric can seem pointless, but it is necessary to make the conformal factor ψ coordinate independent. The resulting coordinate independence makes ψ a scalar tensor field [39]. Although no other restriction is generally imposed to f_{ij}, most implementations consider the background metric to be flat, and we will do so from now on. We can also see that by construction we have

$$det(\tilde{\gamma_{ij}}) = f \ . \tag{38}$$

With this decompositions, the ADM equations 16 and 28 and the constraints become the following system:

$$\left(\frac{\partial}{\partial t} - \pounds_{\boldsymbol{\beta}}\right)\psi = \frac{\psi}{6}\left(\tilde{D}_i\beta^i - \alpha K\right) \tag{39}$$

$$\left(\frac{\partial}{\partial t} - \pounds_{\boldsymbol{\beta}}\right)\tilde{\gamma}_{ij} = -2\alpha\tilde{A}_{ij} - \frac{2}{3}\tilde{D}_k\beta^k\tilde{\gamma}_{ij} \tag{40}$$

$$\left(\frac{\partial}{\partial t} - \pounds_{\boldsymbol{\beta}}\right)K = -\psi^{-4}\left[\tilde{D}_i\tilde{D}^i\alpha + 2\tilde{D}_i ln\psi\tilde{D}^i\alpha\right] + \alpha\left[4\pi\left(u+S\right) + \tilde{A}_{ij}\tilde{A}^{ij} + K^2/3\right] \tag{41}$$

$$\begin{aligned}\left(\frac{\partial}{\partial t} - \pounds_{\boldsymbol{\beta}}\right)\tilde{A}_{ij} = &-\frac{2}{3}\tilde{D}_k\beta^k\tilde{A}_{ij} + \alpha\left[K\tilde{A}_{ij} - 2\tilde{\gamma}^{kl}\tilde{A}_{ik}\tilde{A}_{jl} - 8\pi\left(\psi^{-4}S_{ij} - \frac{1}{3}S\tilde{\gamma}_{ij}\right)\right] \\ &+ \psi^{-4}\Big\{-\tilde{D}_i\tilde{D}_j\alpha + 2\tilde{D}_i\ln\psi\tilde{D}_j\alpha + 2\tilde{D}_j\ln\psi\tilde{D}_i\alpha \\ &+ \frac{1}{3}\left(\tilde{D}_k\tilde{D}^k\alpha - 4\tilde{D}_k\ln\psi\tilde{D}^k\alpha\right)\tilde{\gamma}_{ij} \\ &+ \alpha\Big[\tilde{R}_{ij} - \frac{1}{3}\tilde{R}\tilde{\gamma}_{ij} - 2\tilde{D}_i\tilde{D}_j\ln\psi + 4\tilde{D}_i\ln\psi\tilde{D}_j\ln\psi \\ &+ \frac{2}{3}\left(\tilde{D}_k\tilde{D}^k\ln\psi - 2\tilde{D}_k\ln\psi\tilde{D}^k\ln\psi\right)\tilde{\gamma}_{ij}\Big]\Big\}\end{aligned} \tag{42}$$

$$\tilde{D}_i\tilde{D}^i\psi - \frac{1}{8}\tilde{R}\psi + \left(\frac{1}{8}\tilde{A}_{ij}\tilde{A}^{ij} - \frac{1}{12}K^2 + 2\pi u\right)\psi^5 = 0 \tag{43}$$

$$\tilde{D}_j\tilde{A}^{ij} + 6\tilde{A}^{ij}\tilde{D}_j\ln\psi - \frac{2}{3}\tilde{D}^iK = 8\pi\psi^4 j^i \tag{44}$$

Where eqs (43) and (44) are the constraints of the system and can be rewritten using $\hat{A}_{ij}$ as

$$\tilde{D}_i\tilde{D}^i\psi - \frac{1}{8}\tilde{R}\psi + \frac{1}{8}\hat{A}_{ij}\hat{A}^{ij}\psi^{-7} + \left(2\pi u - \frac{1}{12}K^2\right)\psi^5 = 0 \tag{45}$$

$$\tilde{D}_j\hat{A}^{ij} - \frac{2}{3}\psi^6\tilde{D}^iK = 8\pi\psi^{10}j^i \tag{46}$$

2.3.3 BSSN formulation

The **Baumgarte-Shapiro-Shibata-Nakamura** (BSSN) evolution scheme is a conformal transformation of the ADM equations that further improves the conformal tranformations used by Lichnerowicz and York.
This formulation was developped by Shimata and Nakamura in 1995 [67] and revisited by Baumgarte and Shapiro in 1999 [24] and presents a well-behaved system of equations (unlike the ADM equations). A review on it's hyperbolicity can be seen in [65].

The BSSN formulation diverges from the original conformal tranformation in two aspects:

- The conformal factor ψ i replaced by

$$\phi = \ln\psi = \frac{1}{12}\ln\gamma\ . \tag{47}$$

- Three auxiliary variables are introduced to make the system hyperbolic in nature:

$$\tilde{\Gamma}^i = \tilde{\gamma}^{jk}\tilde{\Gamma}^i_{jk} = -\partial_j\tilde{\gamma}^{ij} \tag{48}$$

where $\tilde{\Gamma}^i_{jk}$ are the Crhistoffel symbols of the conformal metric and the second equality is only true if $\gamma = 1$ (which it is by construction).

With these two new variables, the evolution equations become

$$\partial_t \phi = -\frac{1}{6}\alpha K + \beta^i \partial_i \phi + \frac{1}{6}\partial_i \beta^i \tag{49}$$

$$\partial_t \tilde{\gamma}_{ij} = -2\alpha \tilde{A}_{ij} + \beta^k \partial_k \tilde{\gamma}_{ij} + \tilde{\gamma}_{ik}\partial_j \beta^k + \tilde{\gamma}_{kj}\partial_i \beta^k - \frac{2}{3}\tilde{\gamma}_{ij}\partial_k \beta^k \tag{50}$$

$$\partial_t K = -D_i D^i \alpha + \alpha \left(\tilde{A}_{ij}\tilde{A}^{ij} + \frac{1}{3}K^2 \right) + 4\pi\alpha \left(u + S\right) + \beta^i \partial_i K \tag{51}$$

$$\begin{aligned} \partial_t \tilde{A}_{ij} = {} & e^{4\phi}\left[-\left(D_i D_j \alpha\right)^{TF} + \alpha\left(R^{TF}_{ij} - 8\pi S^{TF}_{ij}\right)\right] \\ & + \alpha\left(K\tilde{A}_{ij} - 2\tilde{A}_{ik}\tilde{A}^k_j\right) \\ & + \beta^k \partial_k \tilde{A}_{ij} + \tilde{A}_{ik}\partial_j \beta^k + \tilde{A}_{kj}\partial_i \beta^k - \frac{2}{3}\tilde{A}_{ij}\partial_k \beta^k \end{aligned} \tag{52}$$

$$\begin{aligned} \partial_t \Gamma^i = {} & 2\tilde{A}^{ij}\partial_j \alpha + 2\alpha\left(\tilde{\Gamma}^i_{jk}\tilde{A}^{kj} - \frac{2}{3}\tilde{\gamma}_{ij}\partial_j K - 8\pi\tilde{\gamma}^{ij}S_j + 6\tilde{A}^{ij}\partial_j \phi\right) \\ & + \beta^j \partial_j \tilde{\Gamma^i} - \tilde{\Gamma}^j \partial_j \beta^i + \frac{2}{3}\tilde{\Gamma}^i \partial_j \beta^j + \frac{1}{3}\tilde{\gamma}^{ki}\beta^j_{,jk} + \tilde{\gamma}^{kj}\beta^i_{,kj} \end{aligned} \tag{53}$$

where $\partial_i \equiv \partial/\partial x^i$ is the covariant derivative associated with the background metric f_{ij} (which is flat) and D_i is the covariant derivative associated with the non-conformal spatial metric γ_{ij}, which can be calculated using the covariant derivative associated with $\tilde{\gamma}_{ij}$ by using the following relation between Christoffel symbols

$$\Gamma^k_{ij} = \tilde{\Gamma}^k_{ij} + 2\left(\delta^k_i \partial_j \phi \delta^k_j \partial_i \phi - \tilde{\gamma}_{ij}\tilde{\gamma}^{kl}\partial_l \phi\right) \ . \tag{54}$$

Because we have added the variables $\tilde{\Gamma}^i$, we also need to add eqs.(48) as a constraint.

Other conformal factors have been also discussed [28, 53] and have been shown to improve the behaviour of the numerical solution near the singularity. Some of this choices include

$$\chi = \gamma^{-1/3} \tag{55}$$

and

$$W = \gamma^{-1/6} \ . \tag{56}$$

In our codes we will use (55), but because the equations are very similar to the BSSN equations for ϕ we will not write them here.

2.4 Initial data

Finding initial data for complex systems is not trivial as we have already commented: On one hand, you need to solve the constraint equations which is already a challenge since in a system of nonlinear and coupled equations. On the other hand, you need the solution to have physical meaning, i.e. to yield a metric that describes the system you are aiming to study.
Most of the methods involve conformal decompositions of the variables as shown in 2.3. The usage of conformal methods was introduced in 1944 by Lichnerowicz [47] and then extended by Choquet-Bruhat in 1956 and 1971 [30, 35], by York and Ó Murchadha in the 1970's with the Conformal transverse-traceless method [59, 78, 80, 83] and in the 2000's by York and Pfeiffer with the so-called Thin Sandwich method [62, 81]. Other approaches not involving conformal decompositions have also been found, but are not as popular in the literature. Therefore we will stick to conformal methods. Recent reviews of the methods can be found in [23, 39, 61].
Although we will not give a full development of the methods, we will try to give an approximate idea on how this methods usually work.

The basic idea is to decompose the metric variables as seen in 2.3, but using the alternative conformal transformation for the traceless extrinsic curvature. We will then have

$$\begin{aligned} &\tilde{\gamma}_{ij} = \psi^{-4}\gamma_{ij} \\ &K = \gamma^{ij}K_{ij} \\ &\hat{A}_{ij} = \psi^{10}A_{ij} = \psi^{10}\left(K_{ij} - \frac{1}{3}\gamma_{ij}K\right) \end{aligned} \tag{57}$$

We will also further decompose $\hat{A}_{ij}$ with a general algebraic result that states that any trace-free symmetric tensor can be decomposed as

$$\hat{A}_{ij} = \hat{A}^*_{ij} + \tilde{D}_i W_j + \tilde{D}_j W_i - \frac{2}{3}\tilde{\gamma}_{ij}\tilde{D}_k W^k \tag{58}$$

where $\hat{A}^*_{ij}$ is a traceless zero-divergence tensor, W_i is a vector and $\tilde{D}_i$ is the covariant derivative associated with the conformal metric.
With this decomposition, the hamiltonian constraint becomes

$$\tilde{D}^2\psi - \frac{1}{8}\psi\tilde{R} - \frac{1}{12}\psi^5 K^2 + \frac{1}{8}\psi^{-7}\hat{A}_{ij}\hat{A}^{ij} = -2\pi\psi^5 u \tag{59}$$

where $\tilde{R}$ is the Ricci scalar associated with the Riemman tensor of the conformal 3-metric.
The momentum constraint becomes

$$\tilde{D}^2 W^i + \frac{1}{3}\tilde{D}^i\tilde{D}_j W^j + \tilde{R}^i_j W^i - \frac{2}{3}\psi^6\tilde{D}^i K = 8\pi\psi^{10} j^i \tag{60}$$

To solve this equations, $\{\tilde{\gamma}_{ij}\ ,\ K\ ,\ \hat{A}^*_{ij}\}$ are given and $\{\psi\ ,\ W_i\}$ are the variables to be found.
Although this two equations should be solved to find initial conditions, they can be heavily simplified with some simple and popular assumptions: The most popular one is to consider the

conformal metric to be flat (this is called **conformal flatness**) and consists on taking

$$\begin{aligned} K &= 0 \\ \tilde{\gamma}_{ij} &= \eta_{ij} \ . \end{aligned} \tag{61}$$

With this assumption, the constraints for vacuum (no matter) become

$$\begin{aligned} \nabla^2\psi + \frac{1}{8}\psi^{-7}\hat{A}_{ij}\hat{A}^{ij} &= 0 \\ \nabla^2 W^i &= 0 \end{aligned} \tag{62}$$

Then the second equation can be easily solved to find W^i, and finally $\hat{A}_{ij}$ is reconstructed to solve for ψ.

As the simplest example of initial conditions, we will consider assume conformal flatness (61 and a moment of time-symmetry, i.e. $K_{ij} = 0$. With this assumptions, the momentum constraint is trivially satisfied and the hamiltonian constraint becomes the Laplace equation

$$\nabla^2\psi = 0 \ . \tag{63}$$

The most simple solution would be $\psi = 1$, which yields the Minkowski metric

$$\gamma_{ij}dx^i dx^j = dx^2 + dy^2 + dz^2 \ . \tag{64}$$

The next possible solution would be

$$\psi = 1 + \frac{a}{r} \tag{65}$$

with a a constant. For $a = m/2$, the spatial metric with spherical coordinates becomes

$$\gamma_{ij}dx^i dx^j = \left(1 + \frac{m}{2r}\right)^4 \left(dr^2 + r^2 d\theta^2 + r^2 sin^2\theta d\phi\right) \ . \tag{66}$$

This is indeed the spatial Schwarzschild metric in isotropic coordinates, which is the physical solution for non-spinning black hole in vacuum.
Because the Laplace equation is linear, we could deduce the initial data for multiple non-spining black holes in vacuum by superposition:

$$\psi = 1 + \sum_i \frac{m_i}{2\|r - r_i\|} \tag{67}$$

2.5 Gauge equations

In section 2.2 we introduced the gauge variables α (lapse) and $\boldsymbol{\beta}$ (shift) and their connection to coordinate choice. We also noted that, although gauge variables appear extensively in the 3+1 formulation of the Einstein equations, those equations don't explain how to choose them or limit in any way the choices we can make. The values for gauge variables are indeed a free choice, which in turn gives us a free choice of coordinates to solve our system. This illustrates perfectly

the coordinate-independent aspect of general relativity theory.

This freedom of choice comes obviously with the question: what actually is the best choice for our gauge variables? A lot of effort has been put over the years to find an answer to this question, and some solutions have been proved to work very well. But the question is still open, specially now that computationally more complicated systems want to be solved. I will not attempt here to give a full detailed explanation on all the gauges that have been tested over the years. I will instead try to give an intuitive explanation on why this is an important issue and how the gauge that our code uses work.
To find a full explanation and development of the most famous gauges, [39] gives a good overview and some examples of where those gauge conditions may be used. Other texts giving reviews of the different gauges choices can be found in [25, 46, 68, 82].

2.5.1 Geodesic gauge conditions

The most intuitive choice one could make would probably be to take

$$\alpha = 1 \tag{68}$$

$$\beta^i = 0 \ . \tag{69}$$

This choice is intuitive because from equation (2) we get that the parametric time (the time in the simulation) becomes the proper time of Eulerian observers and from the definition of the shift we can see that Eulerian observers also become lines of constant spatial coordinates. In fact, Eulerian observers become geodesic lines in this choice of coordinates, which gives the name "geodesic gauge".
In practice, this geodesic gauge conditions give a very bad performance as they don't behave well in presence of singularities (rendering them unusable for black hole computations). The reasons why geodesic conditions don't work for singularities are different in nature for lapse and shift and therefore we will treat them differently.

2.5.2 Lapse moving puncture condition

The most simple case of spacetime with presence of singularity is of course the Schwarzschild metric. If we consider the initial conditions found in 2.4 for the Schwarzschild metric (66) and take the geodesic gauge conditions, we get an initial metric

$$ds^2 = dt^2 + \left(1 + \frac{m}{2r}\right)^4 \left(dr^2 + r^2 d\theta^2 + r^2 sin^2\theta d\phi\right) \ . \tag{70}$$

If we evolve this initial conditions, the code will crash at $t = \pi m$ [39]. The reason is simple if we look at the evolution of the hypersurface, given in figure 2[2].

As we can see, the code crashes because the hypersurface partially touches the singularity (and therefore creates numerical NaN errors). This behaviour is common for geodesic slicing in

[2]Figure taken form [39].

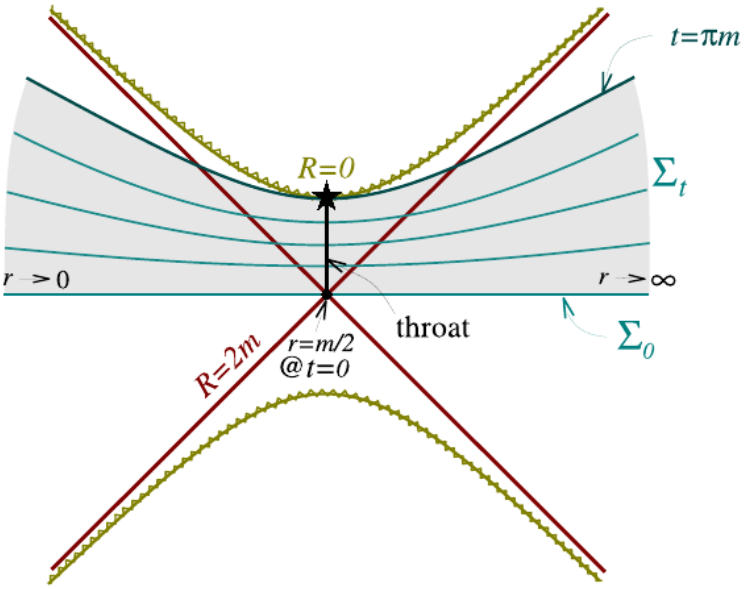

Figure 2: Geodesic-slicing evolution from the initial slice of Schwarzschild spacetime depicted in a Kruskal-Szekeres diagram. R stands for Schwarzschild radial coordinate (areal radius), so that $R = 0$ is the singularity and $R = 2m$ is the event horizon.

presence of singularities, and therefore this type of gauge cannot be used. This problem becomes even more difficult to solve when we start considering black hole binaries, where both black holes are moving (and therefore the punctures move too).

Several lapse conditions have been proposed over the years to solve this problem, but most of them are based on dynamical equations for α that implement **collapse of the lapse** near the punctures. Mathematically, this relies on making α equal to 0 near the punctures, piling up the hypersurfaces close to the singularity so that it is never reached. Physically, this corresponds to freezing Eulerian observer's proper time near the punctures, i.e advancing the simulation only in regions that are far away from the singularity. Indeed, we have seen in 2.2 that

$$d\tau = \alpha dt \ , \tag{71}$$

so if $\alpha = 0$ near some region the simulation can keep going (t increases) without really advancing physical time in that region (τ is fixed). This behaviour can be seen in figure 3[3], where the same initial conditions as in figure 2 are evolved using maximal slicing lapse conditions.

One of the most known way of obtaining this behaviour are maximum slicing lapse conditions, which is obtained by imposing the vanishing of the mean curvature K on all the hypersurfaces Σ_t. This lapse conditions work well, but are generally not used in numerical relativity because they need an elliptic system to be solved at every iteration:

$$D_i D^i \alpha = \alpha \left[4\pi \left(E + S \right) + K_{ij} K^{ij} \right] \tag{72}$$

[3]Figure taken form [39].

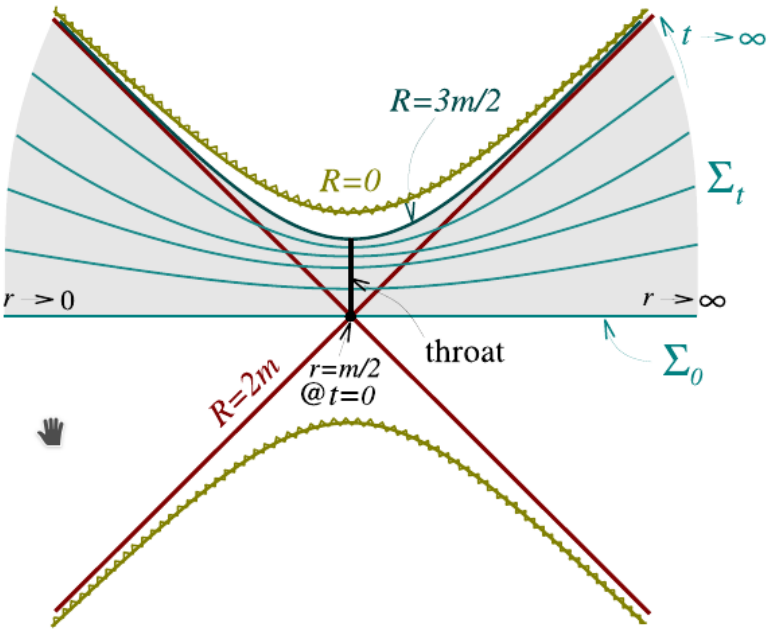

Figure 3: Kruskal-Szekeres diagram depicting the maximal slicing of Schwarzschild spacetime. R stands for Schwarzschild radial coordinate, so that R = 0 is the singularity and R = 2m is the event horizon, whereas r stands for the isotropic radial coordinate.

The lapse conditions that are used in practice are the so-called **1+log slicing conditions**, developed in 1995 by Bona, Massó, Seidel and Stela [27]. They are a generalisation of the **harmonic lapse conditions**, and have the advantage over the maximal slicing that they are written as an evolution equation for α, which is very easily implemented. The general form for the 1+log slicing conditions are

$$(\partial_t - \pounds_{\boldsymbol{\beta}})\,\alpha = -K\alpha^2 f(\alpha) \tag{73}$$

where f is an arbitrary function. Harmonic slicing is obtained with $f(\alpha) = 1$, but taking $f(\alpha) = 2/\alpha$ has been found to have stronger singularity avoidance properties and therefore it is the one used in our code:

$$(\partial_t - \pounds_{\boldsymbol{\beta}})\,\alpha = -2\alpha K \tag{74}$$

2.5.3 Shift moving puncture condition

Shift conditions have historically been less discussed than lapse conditions for the simple fact that in many cases taking $\beta^i = 0$ works just fine. Some numerical problems arise however with the simulation of black hole systems related to grid distortions.
In an intuitive way, one can imagine that black holes "attract" coordinates towards them, distorting the mesh and possibly making it singular after some evolution time. To solve the problem, two shift conditions have historically been implemented that counter this effect.

The first and more intuitive of them is the so-called **minimal distortion shift condition**

[69]. We start by defining

$$\Sigma_{ij} = \frac{1}{2}\gamma^{1/2}\tilde{\gamma}_{ij} \ , \tag{75}$$

which is a measure of how distorted is the mesh at a certain point. Then the condition is simply to impose

$$D^j \Sigma_{ij} = 0 \ . \tag{76}$$

This equation results in a system of coupled elliptic equations that is slow to implement. For that reason, just as we had for the maximal slicing condition, slightly weaker but much faster conditions have been developed and implemented instead.

The conditions used in modern code are called **Gamma-Freezing** or **Gamma-Driver** conditions [16, 29], because they arise from imposing

$$\partial_t \tilde{\Gamma}^k = 0 \ . \tag{77}$$

They mimic the minimal distortion conditions, but are simply implemented with a set of evolution equations for β^i. In their base form, the equations are

$$\begin{aligned} \partial_t \beta^i &= B^i \\ \partial_t B^i &= \partial_t \tilde{\Gamma}^i - \eta B^i \ . \end{aligned} \tag{78}$$

Over the last years this equations have been slightly modified to obtain better behaviours for binary systems [18, 29, 40, 57, 72], notably adding advection terms. The equations we will use in our code will be

$$\begin{aligned} \left(\partial_t - \beta^j \partial_j\right) \beta^i &= \frac{3}{4} B^i \\ \left(\partial_t - \beta^j \partial_j\right) B^i &= \left(\partial_t - \beta^j \partial_j\right) \tilde{\Gamma}^i - \eta B^i \ . \end{aligned} \tag{79}$$

where η is called damping term. This damping term can be taken constant

$$\eta = 2 \ , \tag{80}$$

but in light of recent studies [18, 40, 57] it has been shown the need to make η dependent on the metric, specially for unequal mass simulations (where one of the objects is much more massive than the other one). This has become important since LIGO and LISA are expected to be able to detect star-black hole binaries (that fall in this category), and therefore it is important to increase the precision of simulations in this regard.

2.6 Relativistic Hydrodynamics

In section 2.2 we have studied the 3+1 formalism for the Einstein equations. However, the evolution equations we found for the metric (or geometric) variables must be also coupled with evolution equations for the stress energy tensor $T_{\mu\nu}$, which not only contains information about

regular matter but also about the electromagnetic field.
As a consequence, the complete general treatment of this topic is long and very complicated. However, some cases can be treated quite easily: In this section we will limit ourselves to the case of a **perfect fluid** with no electromagnetic field involved. A more complete treatment on the topic can be found in [39].

In the case of a perfect fluid, the stress energy tensor can be written simply as

$$T_{\mu\nu} = \rho h v_\mu v_\nu + P g_{\mu\nu} \ , \tag{81}$$

where

- ρ is the **rest mass density**,
- P is the **pressure**,
- $h = 1 + \epsilon + P/\rho$ is the **specific enthalpy**,
- ϵ is the **specific internal energy** and
- v^μ is the **fluid 4-velocity**.

The stress-energy tensor must obey two equations for the perfect-fluid case: The first one is the vanishing of it's spacetime divergence, given by the equation

$$\nabla_\mu T^{\mu\nu} = 0 \ . \tag{82}$$

This equation is a consequence of Einstein equations (G is chosen as also having this property) and is general to general relativity. The other equation is more specific to perfect fluids and is the conservation of the baryon number

$$\nabla_\mu \left(\rho v^\mu\right) = 0 \ . \tag{83}$$

To solve this equations numerically, one has to perform a change of variables:

$$D = \rho W \tag{84}$$
$$E = \rho \epsilon W \tag{85}$$
$$S_\mu = \rho h u_\mu W \tag{86}$$
$$V^i = \frac{v^i}{v^0} \tag{87}$$
$$W = \sqrt{-g} v^0 \tag{88}$$

This change of coordinates is a modified version of the 3+1 Eulerian formulation [20, 34] (by

Wilson [75, 76]). With this formulation, the equations for matter become

$$\partial_t D = -\partial_i \left(D V^i \right) \tag{89}$$

$$\partial_t E = -\partial_i \left(E V^i \right) - P \partial_t W - P \partial_i \left(W V^i \right) \tag{90}$$

$$\partial_t S_i = -\partial_j \left(S_i V^j \right) + \frac{S_0}{2} \partial_i g_{00} + S^j \partial_i \beta_j + \frac{S^j S^k}{2 S_0} \partial_i g_{jk} - \sqrt{-g} \partial_i P \tag{91}$$

This equations will be the ones used by the code, although the resulting D, E, S_i and W will then be converted back to ρ, ϵ, P and v^i. Moreover, this dynamical equations will be paired with an equation of state that in the case of the perfect fluid will be

$$P = (\Gamma - 1) \rho \epsilon \ , \tag{92}$$

where Γ is the adiabatic index.

3 An Open-Source Code for Numerical Relativity

Having understood how numerical relativity works from a theoretical point of view, it is important that we also have a brief look at how this theory is implemented. In this section we will briefly introduce the Cactus framework and the Einstein Toolkit, the numerical framework and code library with which our simulations are created. This overview will be both brief and superficial, with the intention of giving a taste on how the code works and, more importantly, acknowledging the work and contributions of dozens of researchers that have been developing this open-source code environment for years. References will be given for whoever wants to explore it more in depth.

3.1 The Cactus Framework

Cactus [1,38] is an open source problem solving environment designed for scientific research and engineer use. It has a modular structure designed to ease customisation and the sharing of code between multiple developers in different programming languages. Cactus offers code parallelisation for running on clusters or supercomputers, but can also be run in personal computers and even laptops for non-research oriented users.

3.1.1 Thorns and Flesh

Cactus gets its name from its design: A central program, called **Flesh**, that coordinates a customizable number of application modules called **Thorns**, that communicate with the central core using a set of predefined functions, variables and files. Although the Flesh is written in Fortran, thorns can be written in multiple programming languages, including C or C++, and run at the same time.
Thorns can be dependent or independent from each other, allowing the construction of bigger toolkits meant to work together or isolated thorns providing more niche utilities.
When the code is built, a separate built tree (referred to as **configuration**) is created for each distinct combination of architecture and configuration options. Associated with each configuration is a list of modules which are actually to be compiled into the resulting executable. This list is called **Thornlist**. Moreover, each version of the executable can be further personalized using a **parameter file** specified at runtime. For instance, each executable could be designed to run a family of systems (black hole binaries, single black holes, binary stars, etc...) which specific parameters can be specified through the parameter file (and made different for each simulation without having to recompile the code).
The role of the flesh can be described by figure 4 [4].

A full list of the thorns provided by the Cactus framework can be found in [3]. A full insight on how the infrastructure works and how thorns can be created and added can be obtained by reading [2,4].

[4] Image taken from [38]

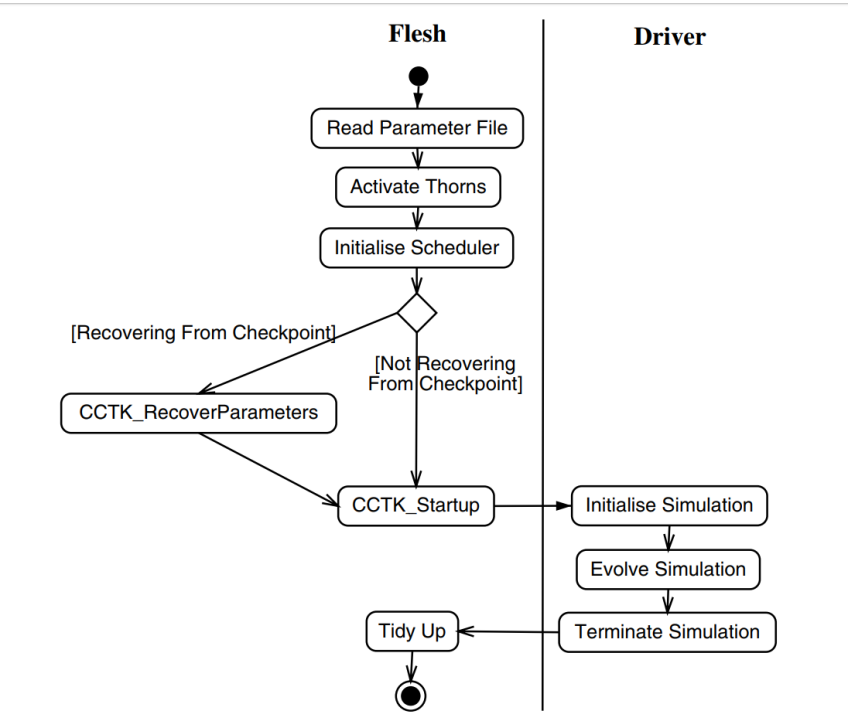

Figure 4: The main flow of control in the Cactus Framework. The flesh initialises the code, then hands control to the driver thorn.

3.1.2 `Carpet`: Adaptative Mesh refinement and interpolation

In Cactus, infrastructure capabilities such as memory management, parallelisation, time evolution, mesh refinement and I/O are controlled by a special component called **driver**. This allows researchers to concentrate on physics and not infrastructure, and makes the hole process more efficient. The Einstein Toolkit has two drivers, `PUGH` and `Carpet`. `PUGH` only provides access to domains with uniform Cartesian grids and it is therefore fallen out of grace in numerical relativity, where mesh refinement is extremely important (more resolution is needed near the punctures).
This features are found in `Carpet` [5], that offers **multi-block methods** and **adaptative mesh refinement (AMR)** [66]. In this subsection we will try to explain what this two concepts are and why they are extremely important for numerical relativity.

Multi-Block methods allow for an arbitrary number of independent grids to be placed around the principal domain grid. Each independent grid (or block) exchanges boundary information with the other grids and the main grid via techniques such as interpolation (see figure 5, down[5]). AMR allows for the resolution in each block to be nonuniform and to be dynamically adapted to the current state of the simulation, such that areas where more precision is needed can have higher resolution. This is done via sets of embedded grids, each one with higher resolution (normally by a factor of two) that it's precedent (see figure 5, up[6]). This grid's hierarchy are called **refinement levels**. At regular intervals, the resolution requirements in the simulation

[5]Image taken from [66]
[6]Image taken from [66]

are re-evaluated and the grid hierarchy is updated.

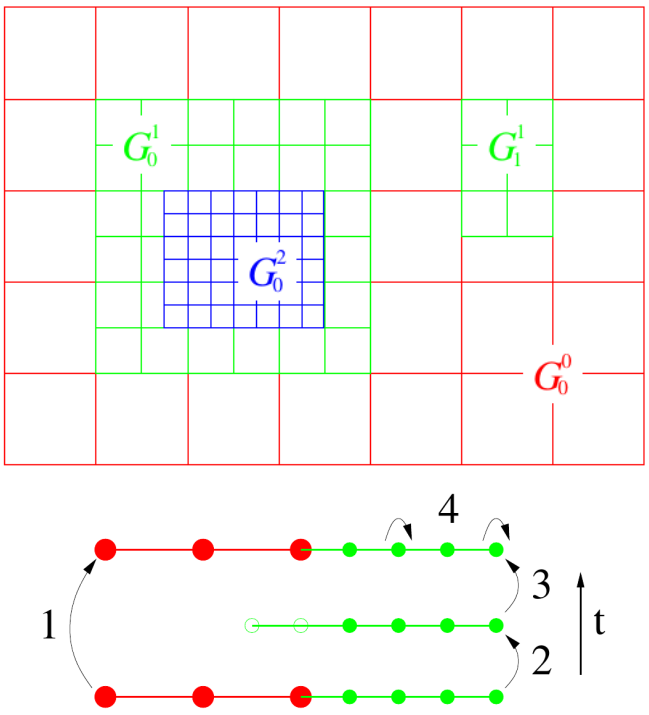

Figure 5: (Up) Base level G_0^0 abd two refinement levels showing the grid alignments and demonstrating proper nesting.
(Down) Schematic for the time evolution scheme, in 1 + 1 dimensions, for a two-grid hierarchy. The large filled red circles represent data on the coarse grid, and smaller filled green circles represent data on the fine grid. The algorithm uses the following order. 1: Coarse grid time step, 2 and 3: fine grid time steps, 4: Copy of shared points (not shown) from fine grid to coarse grid.

The result of combining both this features results in a computational domain with coarse grid, with one or more blocks embedded in it. Each block is a dynamical grid offering further refinement in certain regions, with multiple refinement levels in each block. This blocks can be moved around the coarse grid thanks to AMR, allowing them to always be centered in the regions of interest.

In numerical relativity, one block is usually placed on top of each puncture, with around eight refinement levels (that is a refinement of 2^8 compared to the coarse grid). In case of binary systems, these blocks follow each puncture around the coarse grid as they spiral towards the center.

Without this features, numerical relativity would not be possible, as huge computational domains are needed (so that the gravitational waves computed at the boundaries coincide with the ones we can detect on earth), and the amount of dynamic memory that would be needed to have a homogeneous grid in all that domain (while maintaining the necessary resolution for punctures) would be absurd.

3.1.3 Method of Lines

Another important feature offered by the Cactus framework is the implementation of the time evolution scheme through the **Method of Lines (MoL)** [9,71]. Time evolution is done through finite differences, generally using Runge-Kutta methods of up to fourth order in time.
For finite differences to be implemented, a system of PDEs must be written as an equivalent (up to a certain order) system of ODEs in time

$$\partial_t \boldsymbol{q} = \boldsymbol{L}(\boldsymbol{q}) \tag{93}$$

that can be implemented using standard Runge-Kutta methods. `MoL` offers an interface to implement this method. A variable must be registered, as well as a holder for $\boldsymbol{L}(\boldsymbol{q})$. Then at each iteration the thorn responsible for the evolution of that variable updates $\boldsymbol{L}(\boldsymbol{q})$, which is then used by `MoL` to evolved the variable following the chosen method.
$\boldsymbol{L}(\boldsymbol{q})$ should be computed by external thorns using any arbitrary method (of any chosen order) such as forward, backward or centered differences. This contributes to the modularity of the infrastructure, as different variables may be evolved using different order or different methods that better adapt to the differential equations governing those variables.

3.2 The Einstein Toolkit

The **Einstein Toolkit** [6,50,84] is a collection of thorns for the Cactus framework that offer a complete interface for solving the Einstein equations of gravity in 3+1 formalism, as well as their full implementation. A full list and documentation of the existing thorns can be found in [7].
The thorn collection could be arranged in three main parts:

- **Einstein Base** is the main interface for the implementation of the system equations: it contains very general thorns that should be used in almost every simulation.
  `ADMBase`, `HydroBase` and `TmunuBase` create storage and basic scheduling bins for the ADM variables, the hydrodynamics (Matter) variables and the Stress-Energy tensor respectively.
  `EOS_Base` offers an interface and scheduling bins for the implementation of equations of state.
  All of this thorns do not perform any real action, they just provide a common interface that other thorns can use to evolve the system. This adds to the modularity of the infrastructure.

- **Einstein Initial Data** and **Einstein Evolve** contain respectively thorns that allow setting up the initial data and evolving the system.
  For instance, `GRHydro` is an evolution code for the hydro variables following the scheme presented in section 2.6, and `TwoPunctures` sets up the initial conditions of a binary system of black holes.

- **Einstein Analysis** contains thorns that help with the analysis of the simulation, like tracking the black holes or finding the apparent horizons.

In our simulations, we generally use the `EinsteinBase` thorns, but most if not all of the evolution, initial data and analysis thorns in our runs have been coded by GATech's numerical astrophysics research group over the years. A more detailed explanation of our setup will be given in section 4 for each particular set of simulations.

4 Development of an expanding-universe background for the simulation of black hole binaries

4.1 Introduction and motivation

Like presented in section 1, Numerical Relativity has risen as one of the most prominent ways to study the gravitational waves detected by LIGO. As we wait for the new generation of laser interferometers, the field has to find ways to keep up with the increasing demand in accuracy. It is therefore important to study and tackle all the possible sources of error that the simulations might have.
One of the simplifications numeral relativity codes usually do is to consider the supermassive bodies isolated in an otherwise massless non-expanding universe (a Minkowski background). Although it is a fairly good approximation, it is still physically inaccurate and a potential source of error.

This work aims to start exploring the possibility of new cosmological backgrounds for black hole simulations. Specifically, we consider a particular metric, the Friedmnn-Lemaître-Robertson-Walker (FLRW) cosmology, which, despite being one of the most simple models for an expanding universe, is still seen as a very good approximation. Moreover, the FLRW offers a flat background solution, which makes it suitable to be implemented in our current code without major overhauls.

Throughout this section we will study the FLRW model to then be able to develop the theory necessary to adapt the Cauchy problem presented in section 2 to have an expanding cosmological background. We will then implement this theory into the numerical framework presented in section 3.

4.2 The Friedman-Lemaitre-Robertson-Walker universe

The simplest approach to an expanding cosmology is probably the Friedman-Lemaitre-Robertson-Walker (FLRW) metric. It is an exact solution for the Einstein equations representing an isotropic, homogeneous, path connected and expanding (or contracting) universe. It was developed independently by the four scientists in the 1920's and 1930's and is still today used as a standard model for cosmology, introducing concepts like the **scale factor** and the **Hubble parameter** that are still very much in use today.
The reason for that is because the universe is indeed believed to be both isotropic and homogeneous in sufficiently large scales, i.e. at any point in time the universe looks the same from any point in space and all directions in space are equivalent. For more discussion on this topic, refer to [36, 60, 63, 64].

4.2.1 The FLRW metric

The generic form of the metric, that arises only from the geometric assumptions of isotropy and homogeneity, is the following:

$$ds^2 = -c^2dt^2 + a(t)^2 d\mathbf{\Sigma}^2 \tag{94}$$

where $\mathbf{\Sigma}$ ranges over a 3-dimensional space of constant curvature with no time dependence. All time dependence is included in $a(t)$, which is called the **Scale Factor** and which form is not specified by the geometry assumptions, but by the Einstein field equations as we will discuss in 4.2.2.
One of the most used coordinate systems for the FLRW metric are the polar coordinates $\{r, \theta, \phi\}$, where

$$d\mathbf{\Sigma}^2 = \frac{dr^2}{1 - kr^2} + r^2 \left(d\theta^2 + sin^2\theta d\phi^2\right) \tag{95}$$

Where k is a constant representing the curvature of space. There are a couple of unit choices for k (all other units are adapted as needed), but we will use the following convention: We will take $k \in \{-1, 0, 1\}$ as having no units, which forces r to be also unitless and $a(t)$ to have units of length. This means we will have three very different solutions depending of the value we take for k:

- **For** $k = -1$ we will have an hyperbolic metric, with a universe that is open and that will keep expanding forever.
- **For** $k = 0$ we will have an Euclidean metric, with a universe that is flat and that will eventually neither expand or contract.
- **For** $k = +1$ we will have a parabolic metric, with a universe that is closed and that will eventually collapse.

Many independent measurements seem to indicate that our universe is indeed flat, and the assumption of flatness is also used in inflation theory, which is vastly favoured by scientists as it successfully explains many observations otherwise unexplained. For this reason we will consider $k = 0$ for the rest of the work.
Moreover, with $k = 0$ we can write the metric in Cartesian coordinates:

$$ds^2 = -c^2dt^2 + a(t)^2 \left(dx^2 + dy^2 + dz^2\right) \tag{96}$$

4.2.2 Friedmann equations

As mentioned in 4.2.1, the homogeneity and isotropic conditions do not give a form for the scale factor $a(t)$. This will be given by the Einstein field equations: Using the metric given by 94, we can compute the general expression for the Christoffel symbols. We can then compute the Ricci tensor and scalar. Finally, we will consider the Stress-Energy tensor for the perfect fluid derived in 2.6.
Substituting the mentioned elements into the Einstein field equations, we get to the following

system of equations:

$$\frac{\dot{a}^2 + kc^2}{a^2} = \frac{8\pi G}{3}u \tag{97}$$

$$\frac{\ddot{a}}{a} = -\frac{4\pi G}{3}\left(u + \frac{3P}{c^2}\right) \tag{98}$$

with u and P the energy density and the pressure respectively[7].

This system of equations is know as the **Friedmann Equations** for an isotropic and homogeneous universe. They give us the dynamics of the scale factor a as a function of the energy and mass present in the universe.

Taking the assumption of a flat universe ($k = 0$), $c = G = 1$ as usual and defining the **Hubble Parameter** as

$$H(t) = \frac{\dot{a}}{a}\ , \tag{99}$$

we can rewrite the previous system as

$$H^2 = \frac{\dot{a}^2}{a^2} = \frac{8\pi}{3}u \tag{100}$$

$$\dot{H} + H^2 = \frac{\ddot{a}}{a} = -\frac{4\pi}{3}(u + 3P) \tag{101}$$

which are the Friedmann equations for a flat universe. They will constitute our main tools going forward.

4.2.3 Hubble parameter and Critical energy density

The Hubble parameter as it is defined in 99 is the rate of expansion of our universe. The current rate of expansion, $H_0 := H(t_0)$, is in fact the Hubble constant that appears in the Hubble law. It's value has been calculated for years and therefore is know with great accuracy[8]:

$$H_0 = \frac{h}{9.77\ \text{Gyr}} \quad \text{with} \quad h = 0.6777 \pm 0.013 \tag{102}$$

The fact that this value is known has several consequences. First, it gives us a measurement for the total energy density of our universe: If we consider eq.100, and consider the equation at the present cosmological time t_0, we obtain that

$$u_0 = \frac{3H_0^2}{8\pi} \tag{103}$$

[7]We have omitted here the presence of the cosmological constant, as we will not be considering it in our models and the Friedmann equations with presence of cosmological constant can be reduced to the equations presented here as shown in [32]. Other corrections have also been added to this equations to incorporate more advanced theories like inflation, dark matter or dark energy [32]. None will be treated here.

[8]value measured in 2018 by the Dark Energy Survey collaboration [52]

In fact, if we consider the other two solutions for the FLRW metric we see that for an hiperbolic metric (open universe , $k = -1$) we necessarily have

$$u_0 < \frac{3H_0^2}{8\pi} \ , \tag{104}$$

and for a parabollic metric (closed universe , $k = 1$) we necessarily have

$$u_0 > \frac{3H_0^2}{8\pi} \ , \tag{105}$$

For this reason we define the critical energy density

$$u_{crit} = \frac{3H_0^2}{8\pi} \tag{106}$$

as the energy density necessary in order to have a flat universe.

4.2.4 Exact solutions for the flat FLRW universe

The Friedmann equations can be solved in some simple cases, notably in the case of a perfect fluid, where

$$P = wu \tag{107}$$

with w a dimensionless scalar. In this case, we can combine (100) and (101) to obtain

$$\dot{H} + H^2 = -\frac{4\pi}{3}(u + 3P) = -\frac{1 + 3w}{2}H^2 \ . \tag{108}$$

From here we get

$$\dot{H} = -\frac{3(1 + w)}{2}H^2 \ , \tag{109}$$

that we can integrate in time to obtain ($w \neq -1$)

$$H = \frac{2}{3(w + 1)}t^{-1} \ . \tag{110}$$

Since H depends on the time derivates of a as we have defined in (99), we can further integrate in time to obtain

$$a = \left(\frac{t}{t_0}\right)^{\frac{2}{3(1+w)}} \ , \tag{111}$$

and we define t_0 and $a_0 = a(t_0)$ as the scale factor and the cosmological time at present day. By convention, we will take $a_0 = 1$.

The two most relevant cases for this sort of solution are

- $\boldsymbol{w = 0}$: This would correspond to a pressure-less gas, also called **dust**. This sort of interaction would have been dominant in the earlier stages of the universe. A universe filled with this sort of matter would be called a **matter-dominated universe**.
- $\boldsymbol{w = 1/3}$: This would correspond to a **radiation-dominated universe**, where all the

pressure comes from **radiation pressure**. It is believes that this sort of universe would be dominant later on during the history of the universe.

In our work we will consider we have a radiation-dominated universe, and from now on we will only develop and use this solution, where we have

$$a = \left(\frac{t}{t_0}\right)^{1/2} \tag{112}$$

and considering eq. (110) at present time we get

$$H_0 = \frac{1}{2\ t_0}\ . \tag{113}$$

We can also go back to the first Friedmann equation (100) and substitute our equation for the scale factor, and thus be obtain

$$\frac{(a^{-1}/(2t_0))^2}{a^2} = \frac{8\pi}{3}u\ . \tag{114}$$

From here, we use (113) and (106) to obtain

$$u\ a^4 = u_{crit} \tag{115}$$

which completely determines the evolution of matter in the radiation-driven universe.

4.2.5 Conformal time

We can change the expression of the metric by making a change of coordinates $t \to \eta$ such that

$$ds^2 = a^2(\eta)\left(-d\eta^2 + d\mathbf{\Sigma}^2\right) \tag{116}$$

$$dt = a\ d\eta\ . \tag{117}$$

We will call η the **Conformal Time**, and it's corresponding metric (116) the **Conformal Metric**. This conformal formulation of the FLRW metric will be very useful to develop our gauge conditions in section 4.3.
Equation (117) also allows us to find the Friedmann equations for the conformal time by noticing that

$$a' := \frac{\partial a}{\partial \eta} = \frac{1}{a}\frac{\partial a}{\partial t} = \frac{\dot{a}}{a} \tag{118}$$

and replacing it in (100) and (101). We obtain

$$(a')^2 = \frac{8\pi}{3}ua^4 \tag{119}$$

$$a'' = \frac{4\pi}{3}\left(u - 3P\right)a^3 \tag{120}$$

We can also integrate (117), and we get

$$\eta = \int d\eta = \int a^{-1}\, dt = \int \left(\frac{t}{t_0}\right)^{-1/2} dt = 2\, t_0 \left(\frac{t}{t_0}\right)^{1/2} . \tag{121}$$

We can evaluate this equation at present time to obtain

$$\eta_0 = 2\, t_0 \tag{122}$$

and then we can use this to get the scale factor as a function of the conformal time

$$a = \eta/\eta_0 \tag{123}$$

4.3 Development of the gauge conditions

After studying the background we want to implement, we can start tackling the actual problem we were set to solve: Finding lapse conditions for this sort of background.
First, we should take a look to the conformal metric for the flat FLRW universe

$$ds^2 = -a^2 d\eta^2 + a^2 \left(dx^2 + dy^2 + dz^2\right) \tag{124}$$

and compare it to the conformal 3+1 metric with null shift ($\beta^i = 0$)

$$ds^2 = -\alpha^2 dt^2 + \chi \tilde{\gamma}_{ij} dx^i dx^j . \tag{125}$$

It is then clear that we could reproduce a flat FLRW universe with conformal metric by making the associations

$$\begin{aligned} \eta &\equiv t \\ a &\equiv \alpha \\ a^2 &\equiv \chi \\ \tilde{\gamma}_{ij} &\equiv \eta_{ij} \end{aligned} \tag{126}$$

where η_{ij} is the Minkowski metric. We can then consider two approaches to get lapse conditions:

- We can consider the first conformal Friedmann equation (119) and use (115) to get

$$(a')^2 = \frac{8\pi}{3} u_{crit} , \tag{127}$$

  and use our definition for U_{crit} (106) to obtain

$$(a')^2 = H_0^2 , \tag{128}$$

  which of course brings us to

$$\partial_t \alpha \equiv a' = H_0 . \tag{129}$$

This will be the our first option for our lapse condition.

- We can also consider the BSSN evolution equation for the conformal factor (without the advection term because $\beta^i = 0$)
$$\partial_t \chi = -\frac{1}{6}\alpha\chi K \tag{130}$$
and then replace the conformal factor by it's association to get
$$2aa' = -\frac{1}{6}\alpha a^2 K \ , \tag{131}$$
which becomes
$$\partial_t \alpha = -\frac{1}{3}\alpha^2 K \ . \tag{132}$$
This equation will be our second option for our lapse condition.

In fact, and most naturally, both equations (129) and (132) are the same. Indeed, if we calculate the extrinsic curvature for the FLRW universe (app. A , (169)) we have that

$$K = 3H = -3H_0 a^{-2} \tag{133}$$

Note that the second equality only holds in conformal time. From here we substitute in (132) to obtain (129).

It also needs to be noted that (132) is a 1+log lapse condition as presented in section 2.2.1 by taking
$$f(\alpha) = 1/3 \ . \tag{134}$$
For that reason we will use the form (132) in the code. However, this lapse condition is not fit for puncture evolution. Indeed it does not achieve collapse of the lapse ($\alpha = 0$) in the punctures. For that reason we will implement a convex combination between the moving punctures lapse equation (74) and (132) such that the evolution follows (74) at the punctures and (132) near the boundary. We will also apply a correction to (74) to account for the different value K takes in the FLRW metric.

The lapse we will implement will therefore be

$$\begin{aligned}\left(\partial_t - \beta^i\partial_i\right)\alpha = &-2\left[0.5 - 0.5\,\tanh\left(\frac{r-R_0}{\sigma}\right)\right]\alpha\left(K+3H\right)\\ &-\frac{1}{3}\left[0.5 + 0.5\,\tanh\left(\frac{r-R_0}{\sigma}\right)\right]\alpha^2 K \ ,\end{aligned} \tag{135}$$

which corresponds to a 1+log lapse with

$$\begin{aligned}f(\alpha) = 2\alpha^{-1}&\left[0.5 - 0.5\,\tanh\left(\frac{r-R_0}{\sigma}\right)\right]\left(\frac{K+3H}{K}\right) +\\ &\frac{1}{3}\left[0.5 + 0.5\,\tanh\left(\frac{r-R_0}{\sigma}\right)\right]\end{aligned} \tag{136}$$

4.4 Development of the boundary conditions

An important part of every Cauchy problem are boundary conditions, which impose analytical solutions in the simulation boundary. In numerical relativity, it is assumed that the integration domain is big enough so that the black holes present around the origin do not influence the solution at the boundaries. Therefore the values we will impose at the boundaries will be the analytical values for the background, in our case the FLRW metric.

4.4.1 Hydro boundary conditions

As we have seen in section 2.6, our code for matter uses the rest mass density ρ, the intrinsic internal energy ϵ, the pressure P and the 4-velocity v^μ to calculate the evolution of matter. It is then necessary to calculate boundary conditions for this variables.
This process somewhat more complicated than it seems because of the fact that our model only provides an analytic solution for the energy density u and not the variables we actually need.
First, we will consider that we are in a co-moving frame with the fluid, i.e.

$$v^0 = 1 \quad , \quad v^i = 0 \ . \tag{137}$$

We will then consider the equation implemented equation of state: For a perfect fluid we will use the equation of state given by (92), using $\Gamma = 4/3$ because we want our matter to be radiation (we need $\Gamma - 1 = 1/3$). This gets us to the following equation of state

$$P = \frac{1}{3}\rho\epsilon \ . \tag{138}$$

Finally we only need boundary conditions for ρ and ϵ. These will be given by the following system of equations:

$$\begin{aligned} u &= \rho(1+\epsilon) \ , \\ \epsilon &= \frac{K_\epsilon}{\Gamma - 1}\rho^{\Gamma-1} = 3K_\epsilon\rho^{1/3} \ , \end{aligned} \tag{139}$$

where the first is only a definition and the second equation is the standard way to calculate ϵ in the code. K_ϵ is a constant that is usually taken with a value of 100. If we combine both equation taking into account that u is known, and introduce equation (115) we get that

$$\begin{aligned} \rho &= \frac{u_{crit}}{(1+\epsilon)a^4} \\ \epsilon^3(1+\epsilon) &= 27K^3 u_{crit} a^{-4} \end{aligned} \tag{140}$$

The second equation cannot be solved analytically, so in the code we implement a Newton-Raphson method to calculate the value of ϵ at every time step. The initial conditions for the algorithm are motivated by Taylor expansions of the target function:

$$\begin{aligned} \epsilon_0 &= \left(27K^3 u_{crit} a^{-4}\right)^{1/4} \quad \text{for} \quad \left(27K^3 u_{crit} a^{-4}\right)^{1/4} \geq 0.5 \\ \epsilon_0 &= \left(27K^3 u_{crit} a^{-4}\right)^{1/3} \quad \text{for} \quad \left(27K^3 u_{crit} a^{-4}\right)^{1/4} < 0.5 \end{aligned} \tag{141}$$

Once the boundary value for ϵ is obtained, the value for ρ is recovered from the first equation in (140).

4.4.2 Metric boundary conditions

To obtain the metric boundary conditions we only have to use what we have already learned about the FLRW metric in conformal time:

$$\begin{aligned} \chi &= a^2 \\ \tilde{\gamma_{ij}} &= \eta_{ij} \\ K &= -3H_0 a^{-2} \\ \tilde{A}_{ij} &= 0 \end{aligned} \tag{142}$$

However, we do not want to have Dirichlett boundary conditions because of numerical errors introduced by reflections at the boundaries. Instead, we need to create reflection-absorbing boundary conditions [16,17]. We consider any scalar variable (or tensor component) f such that

$$f(x^i, t) = f_0 + \frac{u(r-t)}{r} \ , \tag{143}$$

i.e that f is composed of a base function f_0 and a wave-like distortion u that fades as $1/r$. Physically, f_0 will be our background value and u is the distortion created by the black hole(s) at the center of the the simulation domain.
Note that we consider u spherically symmetric, which is not true for black hole binaries and other asymmetric systems. However, we are considering ourselves at the boundaries which are supposed to be "infinitely far away" from the observed system, so spherical symmetry is a good approximation.

Because simulations are done generally with a Minkowski background, that is not dependent on time, the boundary conditions consider f_0 to be constant in time. We will thus need to develop our own variation of reflection-absorbing boundary conditions.
We start by considering the time and space derivatives of (143):

$$\partial_t f = \partial_t f_0 - \frac{u'(r-t)}{r} \tag{144}$$

$$\partial_i f = -\frac{x^i}{r^3} u(r-t) + \frac{x^i}{r^2} u'(r-t) \tag{145}$$

where we have used that

$$\begin{aligned} &\frac{\partial r}{\partial x^i} = \frac{x^i}{r} \ , \\ &\partial_i u(r-t) = \frac{\partial r}{\partial x^i} \frac{\partial u(r-t)}{\partial r} = \frac{x^i}{r} u'(r-t) \ . \end{aligned} \tag{146}$$

Then we have that

$$\begin{aligned}\frac{x^i}{r^2}(f-f_0) &= \frac{x^i}{r^3}u(r-t)\\ &= -\partial_i f + \frac{x^i}{r^2}u'(r-t)\\ &= -\partial_i f - \frac{x^i}{r}\partial_t f + \frac{x^i}{r}\partial_t f_0\end{aligned} \tag{147}$$

and from this last equation we can reorder the terms to obtain

$$\begin{aligned}\partial_t f &= \partial_t f_0 - \frac{f-f_0}{r} + \frac{r}{x^i}\partial_i f\\ &= \partial_t f_0 - \frac{f-f_0}{r} + \frac{\partial x^i}{\partial r}\partial_i f\end{aligned} \tag{148}$$

which is a differential equation for f that can be implemented as boundary conditions.
This last expression can also be generalised to obtain

$$\partial_t f = \partial_t f_0 - \frac{f-f_0}{r} + \partial_r f \ . \tag{149}$$

We will implement this boundary conditions for all the metric variables $\{\tilde{\gamma}_{ij}, \chi, K, \tilde{A}_{ij}, \tilde{\Gamma}^i\}$ taking f_0 as the analytical value given by (142).

4.5 Development of the initial data

Another important aspect we had to develop where the initial conditions for our Cauchy problem. For this project we developed two sets of initial conditions: one set for pure cosmological simulations (without punctures) and another for simulation of punctured space-times (which is our final objective).

4.5.1 Cosmological simulations

For cosmological simulations we aim to reproduce the flat FLRW metric for a radiation-dominated universe. The initial data will therefore be very similar to the boundary conditions we just built simply taking $t = \eta_0$ (here t is not the cosmological time but the simulation time parameter). For the metric initial data, however, the variables to be set will not be the BSSN variables but rather the ADM variables $\{\gamma_{ij}, K_{ij}, \alpha, \beta^i\}$.
The initial conditions for the hydro variables will be given by

$$\begin{aligned}v_0^i &= 0\\ \rho_0 &= \frac{u_{crit}}{(1+\epsilon_0)a_0^4}\\ \epsilon_0^3(1+\epsilon_0) &= 27K^3 u_{crit} a_0^{-4}\\ P_0 &= \frac{1}{3}\rho_0\epsilon_0\end{aligned} \tag{150}$$

The initial conditions for the metric variables will be given by

$$\begin{aligned} \gamma_{ij} &= a_0^2 \eta_{ij} \\ K_{ij} &= -a_0^2 H_0 \delta_{ij} \\ \alpha &= a_0 \\ \beta^i &= 0 \end{aligned} \tag{151}$$

All the above quantities depend on the initial values a_0 , H_0 and η_0 that we can set using equations 112, 113 and 122: if we take $a_0 = 1$ by convention, then

$$H_0 = \frac{1}{2t_0} = \frac{1}{\eta_0} \ . \tag{152}$$

For convenience, we will choose to start our simulations at $t = 1$, so we have to impose $\eta_0 = 1$, and then we get that $H_0 = 1$.

4.5.2 Puncture simulations

As discussed in section 2.4, finding initial data for Black hole simulations is not trivial and involves solving a system of coupled elliptic equations. We alsoo saw that is we assume $\tilde{R}_{ij} = K = u = 0$ we get to a much easier system that is easily solved. Although for a FLRW metric two of those assumptions cannot be made, we can work around this problem if we take a closer look to the equations.

First, let's consider the Hamiltonian equation taking into account that in our case $\tilde{\gamma}_{ij} = \eta_{ij}$ (i.e $\tilde{R}_{ij} = 0$):

$$\nabla^2 \psi - \frac{1}{12}\psi^5 K^2 + \frac{1}{8}\psi^{-7}\hat{A}_{ij}\hat{A}^{ij} = -2\pi\psi^5 u \tag{153}$$

If we consider the matter term, and develop it using the FLRW metric equations at $t = \eta_0$, we get that

$$-2\pi\psi^5 u = -2\pi\psi^5 u_{crit} = -2\pi\psi^5 \frac{3H_0^2}{8\pi} = -\frac{3}{4}\psi^5 \left(-\frac{1}{3}K\right)^2 = -\frac{1}{12}\psi^5 K^2 \tag{154}$$

So our Hamiltonian equation becomes

$$\nabla^2 \psi + \frac{1}{8}\psi^{-7}\hat{A}_{ij}\hat{A}^{ij} = 0 \tag{155}$$

which is equivalent to solve the Hamiltonian equation with $K = u = 0$.

In the same spirit, we can consider the Momentum constraint

$$\tilde{D}^2 W^i + \frac{1}{3}\tilde{D}^i \tilde{D}_j W^j - \frac{2}{3}\psi^6 \tilde{D}^i K = 8\pi\psi^{10} j^i \tag{156}$$

and we can see that

- because of K being constant in space, we have $\tilde{D}^i K = 0$

- and if we develop j^i we have that

$$j^i = \left(\delta^i_\mu + n^i n_\mu\right)\left(n_\nu T^{\mu\nu}\right) = n_\nu T^{i\nu} + n^i u \tag{157}$$

  and considering the expressions for n^μ and n_μ as well as $\beta^i = 0$ we have that $j^i = 0$.

In the end, like with the Hamiltonian constraint, we will have that the Momentum equation that we want to solve is equivalent to the $K = u = 0$ case.

This is very important because it will allow us to use extremely well-optimised already existing code to solve our initial constraints. Indeed, we will proceed as follows:

- First, we will use the already-existing code to solve the constraints for the case $K = u = 0$. This will yield values for A_{ij} and ψ corresponding to a puncture space without matter and conformally flat.

- During the construction of the ADM variables using the computed values, we will use our analytical solutions for K and matter to create the actual initial data as follows:

$$\begin{aligned} \gamma_{ij} &= a_0^2 \psi^4 \eta_{ij} \\ K_{ij} &= A_{ij} + \frac{1}{3}\gamma_{ij} K = A_{ij} - H_0 \gamma_{ij} \end{aligned} \tag{158}$$

- We will add our hydro initial conditions as given by equations (150).

Because of what we have seen in this section, we know this new data will also be solution of the constraint equations, so our simulation can start without any trouble. Like for the cosmological simulations, we will use $a_0 = \eta_0 = H_0 = 1$ as our initial cosmological constants.

4.6 Numerical simulations

After the theoretical development of sections 4.3, 4.4 and 4.5, we should be able to implement the background into our puncture simulations.
To this purpose, we have coded two thorns:

- `FLRWBackground` is a thorn that has two main functions: First, it interacts with `ADMBase` and `HydroBase` to set the initial conditions for the metric and the hydro variables (separately). Second, it provides boundary conditions for the hydro variables that follow the theory developed in section 4.4.1.

- `TwoPuncturesFLRW` is a thorn modified from our own version of the EinsteinToolkit thorn `TwoPunctures`. `TwoPunctures` solves the Hamiltonian and Momentum constraints for a conformaly flat universe without matter using a single domain spectral method [21]. We have modified it to create our metric initial data for punctures, following the methodology developed in section 4.4.2.

4.6.1 Radiation-dominated FLRW flat cosmology in conformal time

As a first result, and to test both our theoretical development and code, we have performed a simulation of a flat and radiation-dominated FLRW universe. This work can be seen as a radiation-dominated counterpart of the matter-dominated FLRW universe found in [26].

For this runs, we will evolve the initial data provided by `FLRWBackground` (both metric and hydro) using our own implementation of the BSSN system [9] paired with `GRHydro` [55] for the evolution of the hydro variables. We use fourth order finite differencing for the metric variables and second order diferencing for the hydro variables.
We use the PPM reconstruction method [31] and the Riemann solver Marquina [43], both coded into `GRHydro`, to convert the conserved hydro variables E, D, S_i, V^i back to the primitive variables and solve the evolution system (89).
We use `EOS_Base` and `EOS_Omni` to implement the equation of state (138).
As gauge conditions, we use constant shift and our lapse condition (129) that we code into our BSSNOK evolution code. For the boundary conditions, we also modify our evolution thorn to provide the metric boundary conditions seen in (142) using the dynamic implementation seen in (149). The hydro boundary conditions will be implemented using `FLRWBackground`.

For simulation domain, we have taken a cartesian grid with a single level of refinement and without imposing any symmetry. We introduce two parameters L and Δ such that the domain boundaries and the point separation can be written as

$$\begin{aligned} x^i &\in [-L, L] \\ \Delta_i &= \Delta \cdot L \end{aligned} \tag{159}$$

We will also consider the time-step Δ_t.
The only other parameters our simulation has are the already discussed a_0 , H_0 and t_0, which respectively the initial scale factor, Hubble parameter and cosmological time.

We have taken for this parameters

$$\begin{aligned} L = 10 \ , \quad \Delta = 0.05 \ , \quad \Delta_t = 0.5 \cdot 2^{-5} \ , \\ a_0 = 1 \ , \quad H_0 = 1 \ , \quad t_0 = 1 \end{aligned} \tag{160}$$

We evolve the system from $t = t_0\mathcal{M}$ to $t = 45\mathcal{M}$, and the results can be found in figure 6 and 7, that show the evolution of some variables and their errors respect of the analytical solutions respectively. The three variables have been chosen because they represent the system fully:

- *chi* represents fully the evolution of the spacial metric, since the conformal metric is flat (both in theory and in our simulation). Moreover, because of (142) we have that *chi* is closely related to the scale factor $a(t)$ and therefore correct evolution can be induced by the correct evolution of χ.

[9] Coded using Kranc [8, 42]

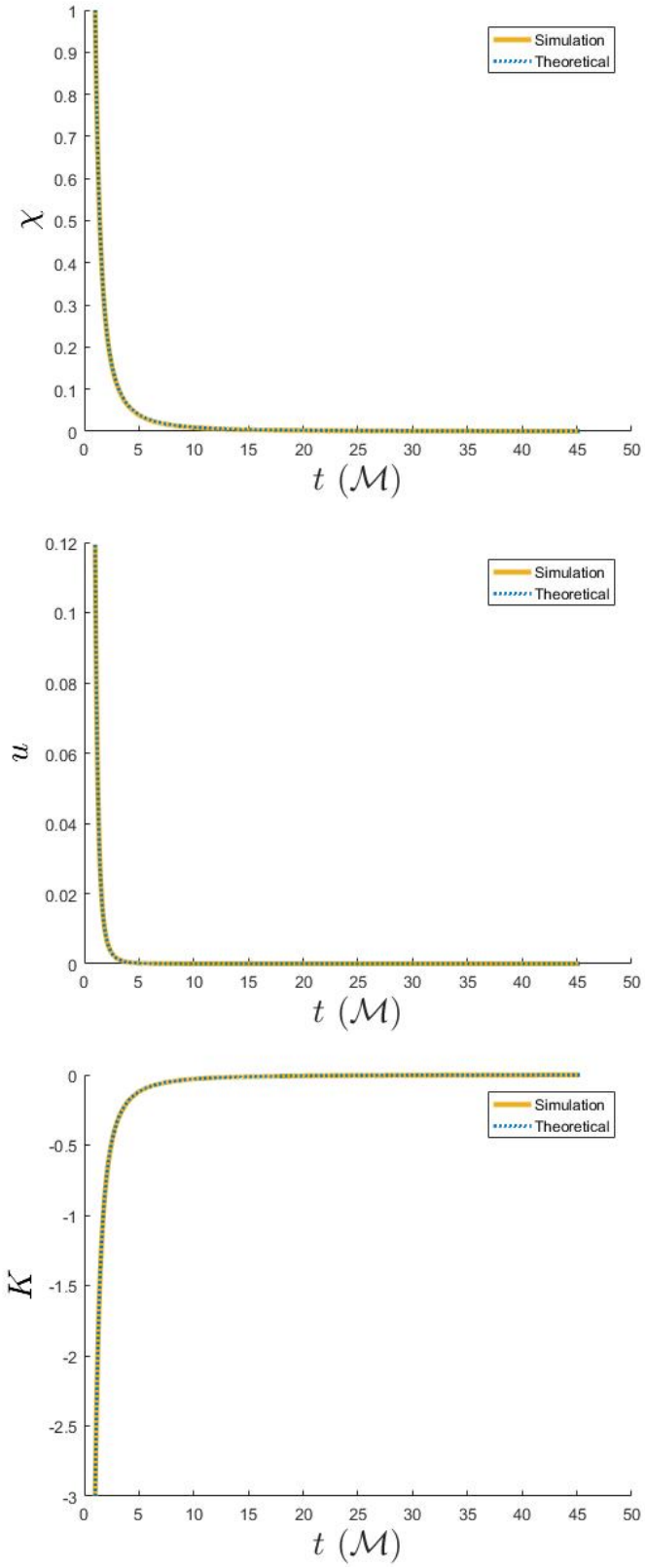

Figure 6: Evolution of χ (top left) , u (top right) and K (bottom) obtained through the simulation of a flat and radiation-dominated FLRW universe. In every case, the data is paired with a dotted curve showing the analytical evolution of that variable.

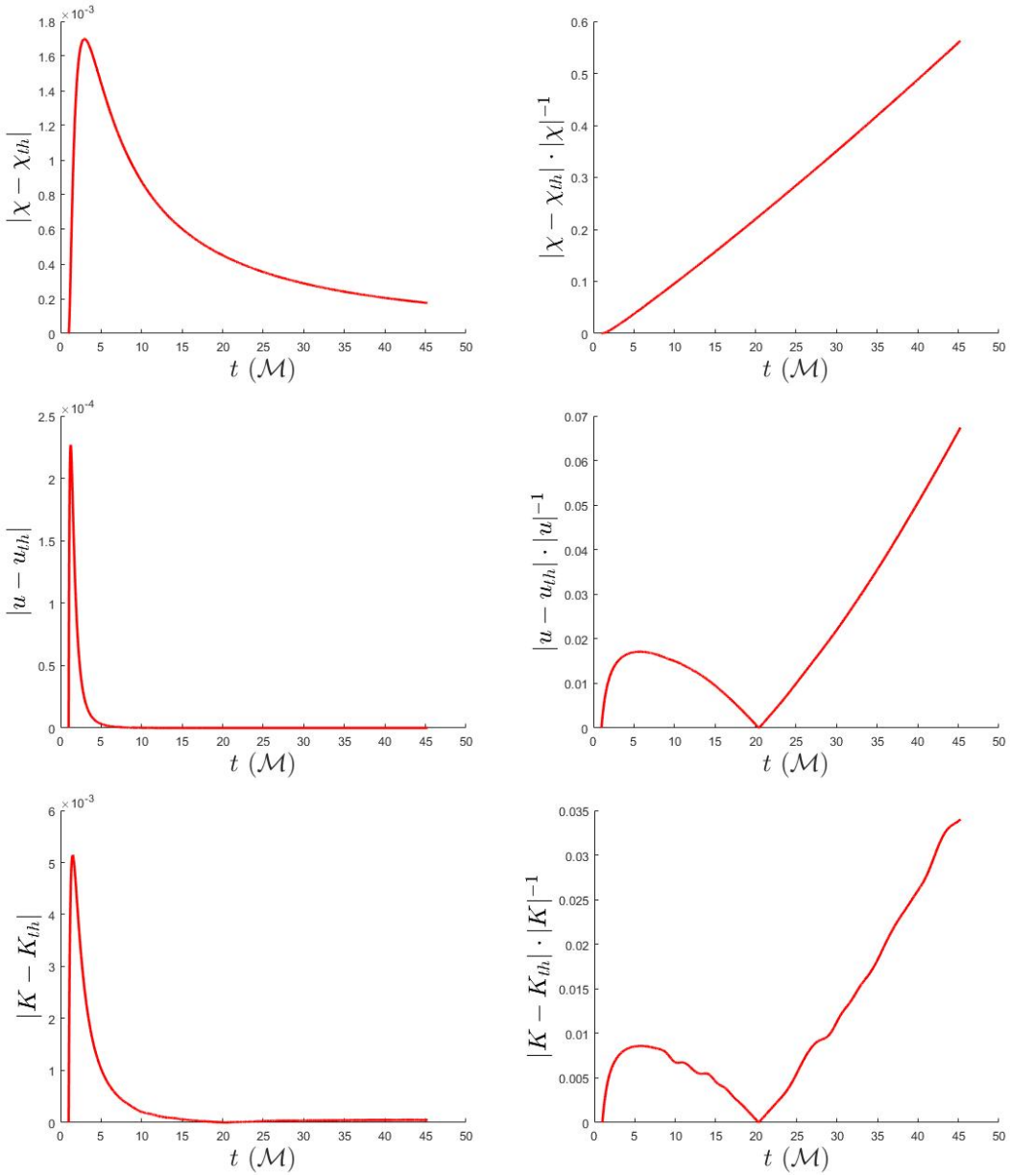

Figure 7: Error plots for χ (top) , u (middle) and K (bottom) obtained through the simulation of a flat and radiation-dominated FLRW universe. For every variable, we have the absolute error (left) and the relative error (right).

- K represents fully the extrinsic metric, because the traceless curvature A_{ij} is null and remains null throughout the evolution. Moreover, K also gives the evolution of the Hubble parameter $H(t)$ because of (169).
- u represents fully the matter, because it is a nontrivial combination of ρ and ϵ and the evolution of P is imposed by the equation of state from the evolution of those two variables.

Looking at figure 6, we can see the theoretical curve fits beautifully the evolved data.

However, to better appreciate the magnitude of the errors we have to take a look at figure 7. For the three variables we have on the left the absolute error and on the right the relative error. We can clearly see that K and u have much better results than χ. Their relative error stays under 1% during the whole simulation. It is significantly worse for χ, where the relative error gets to 7%.
The other significant observation is that the relative error seems to keep augmenting as the simulation progresses. This is normal with numerical methods, and could further be justified by the fact that the rate of change of the variables slows down progressively, so floating point errors become more important.

4.6.2 Non-spining black hole in a radiation-dominated FLRW flat background

The second step would be to test our puncture-designed gauge equations with the simplest metric containing punctures. This corresponds to the case of a single non-spining black hole, also known as the Schwarzschild metric.

For this runs, we evolve the initial data provided by `FLRWBackground` (hydro) and `TwoPuncturesFLRW` (metric) using our own implementation of the BSSN system [10] paired with `GRHydro` [55] for the evolution of the hydro variables. We use fourth order finite differencing for the metric variables and second order diferencing for the hydro variables.
We use the PPM reconstruction method [31] and the Riemann solver HLLE [74], both coded into `GRHydro`, to convert the conserved hydro variables E, D, S_i, V^i back to the primitive variables and solve the evolution system (89).
We use `EOS_Base` and `EOS_Omni` to implement the equation of state (138).
As gauge conditions, we use constant shift and our lapse condition (132) that we code into our BSSNOK evolution code. For the boundary conditions, we also modify our evolution thorn to provide the metric boundary conditions seen in (142) using the dynamic implementation seen in (149). The hydro boundary conditions will be implemented using `FLRWBackground`.

Unfortunately we have not yet been capable of successfully evolving our initial conditions: Although the initial conditions are set as we need them to be, we are having big problems evolving the hydro variables at the puncture. This problem is known and has nothing to do with the

[10] Coded using Kranc [8, 42]

physics. It is purely a numerical problem that we are currently trying to solve.
This is also a know problem that has been solved in [74]. The numerical fix is known as 'Faber Trick' in reference to the author and is normally implemented in `GRHydro`. We have however been unsuccessfully so far trying to use it.

A possible explanation is the fact that so far (and to our our knowledge) thi strick has been used to evolve both neutron starts and black holes with Bondi accretion. The first has high density but it is not a real puncture, whereas the second is a puncture but has very low density near it. We therefore think at this moment that the problem we are experiencing is caused by our punctured space-time paired with high densities. This densities are due to our choice of parameters a_0, H_0 and t_0, and one option we will definitely explore in the future is trying to reparametrize (basicaly rescale) our system so that such high densities are not obtained near the puncture.
Another option could be to try to find a more stable thorn for the evolution of the hydro variables: `GRHydro` is the free version of a more complex code named `Whisky` [10] that is in constant improvement and could have better stability that it's open-source counterpart. We have also access to the hydro thorn developed by the Illinois Numerical Relativity Group [33, 58]. The later is preferred by some of our colleagues working with neutron stars as it is believed by them to be more stable. However, this code does not support symmetries yet and it is therefore a lot more costly to implement (both in computational time and more importantly RAM).
In any case, progress on this matter is supposed to be made in the near future.

5 Conclusions & Further work

We have explored how the Einstein equations have been treated to obtain a formulation suitable for their numerical implementation. We have also discussed the problems that arise throughout the process and have given the state-of-the-art solutions that are currently being used in the field of Numerical Relativity.
We have presented an open-source code, the Cactus framework and the Einstein Toolkit, that is being used and developed by Numerical Relativity groups around the world to implement the Einstein equations.
We have also developed the theory for a new and more physically accurate background, the Friedmann-Lemaître-Robertson-Walker metric, which is a homogeneous, isotropic, flat and expanding universe.
Finally, we have successfully simulated this metric on it's own and are close to successfully evolve a single non-rotating puncture with this new background.

In the near future, we aim to finish implementing the single-puncture simulation. Once that is done, the next objective would be to successfully evolve a system that is able to produce gravitational waves, like a black hole binary. This would allow us to achieve the real goal of this project, which is to study how the assumption of a Minkowski background is affecting our simulations (if it is) and quantify error introduced (if there is any).
This would bring the Numerical Relativity community a step closer to understanding all the possible sources of error in the simulations and therefore be able to keep up with the increase in precision that will be necessary in the future when better Gravitational Wave detectors come into play.

A Extrinsic curvature for the FLRW metric

We will calculate the extrinsic curvature using the FLRW metric in cosmological time, so we will have

$$\begin{aligned} g_{\mu\nu} &= \begin{pmatrix} -1 & 0 \\ 0 & a^2\eta_{ij} \end{pmatrix} \\ n^\nu &= \begin{pmatrix} 1 & 0 & 0 & 0 \end{pmatrix} \\ n_\nu &= \begin{pmatrix} -1 & 0 & 0 & 0 \end{pmatrix} \end{aligned} \tag{161}$$

The extrinsic curvature is given eq.(12)

$$\begin{aligned} K_{\mu\nu} &= -\nabla_\mu n_\nu - n_\mu n^\epsilon \nabla_\epsilon n_\nu \\ &= -\partial_\nu n_\nu + \Gamma^\epsilon_{\mu\nu} n_\epsilon - n_\mu n^\epsilon \partial_\epsilon n_\nu + n_\mu n^\epsilon \Gamma^\lambda_{\epsilon\nu} n_\lambda \\ &= \Gamma^\epsilon_{\mu\nu} n_\epsilon + n_\mu n^\epsilon \Gamma^\lambda_{\epsilon\nu} n_\lambda \\ &= -\Gamma^0_{\mu\nu} - n_\mu \Gamma^0_{0\nu} \end{aligned} \tag{162}$$

We therefore have to calculate the Christoffel symbols of the form $\Gamma^0_{\mu\nu}$, that are given by

$$\Gamma^\mu_{\alpha\beta} = \frac{1}{2} g^{\mu\nu} \left[\frac{\partial g_{\alpha\nu}}{\partial x^\beta} + \frac{\partial g_{\beta\nu}}{\partial x^\alpha} - \frac{\partial g_{\alpha\beta}}{\partial x^\nu} \right] \tag{163}$$

Because most of $g_{\mu\nu}$ is constant, we have that

$$\Gamma^\mu_{\alpha\beta} = -\frac{1}{2} \frac{\partial g_{\alpha\beta}}{\partial t} \tag{164}$$

It is then trivial to see that

$$\Gamma^0_{00} = \Gamma^0_{i0} = \Gamma^0_{0i} = 0 \tag{165}$$

$$\Gamma^0_{ij} = \dot{a} a \ \delta_{ij} \tag{166}$$

Using this expressions we can now calculate the values for $K_{\mu\nu}$: We can first see that

$$K_{00} = K_{i0} = K_{0i} = 0 \tag{167}$$

as we expect since it should be a purely spatial tensor. We can also get that

$$K_{ij} = -\dot{a} a \ \delta_{ij} = -a^2 H \ \delta_{ij} \tag{168}$$

Finally, we will also obtain the expression for the trace of the extrinsic curvature, which will be given by

$$K = \gamma^{ij} K_{ij} = \left(a^{-2} \ \eta_{ij} \right) \left(-a^2 H \ \delta_{ij} \right) = -3H \tag{169}$$

References

[1] Cactus computational toolkit home page:. http://cactuscode.org.

[2] Cactus reference manual:. https://www.cct.lsu.edu/~gallen/Reports/Cactus_ReferenceManual.pdf.

[3] Cactus thorn guide:. https://www.cct.lsu.edu/~gallen/Reports/Cactus_ThornGuide.pdf.

[4] Cactus users guide:. https://www.cct.lsu.edu/~gallen/Reports/Cactus_UsersGuide.pdf.

[5] Carpet driver homepage:. https://carpetcode.org/.

[6] Einstein toolkit home page:. http://einsteintoolkit.org.

[7] Einstein toolkit thorn documentation:. https://einsteintoolkit.org/documentation/ThornGuide.php.

[8] Kranc code homepage:. http://kranccode.org/.

[9] Mol reference manual:. https://www.cct.lsu.edu/~goodale/Teaching/KISTI/MoL.pdf.

[10] Whisky code homepage:. http://www.whiskycode.org/.

[11] J. Aasi, J. Abadie, B. P. Abbott, R. Abbott, T. D. Abbott, M. Abernathy, T. Accadia, F. Acernese, C. Adams, T. Adams, P. Addesso, R. Adhikari, C. Affeldt, M. Agathos, K. Agatsuma, P. Ajith, B. Allen, A. Allocca, E. Amador Ceron, D. Amariutei, S. B. Anderson, W. G. Anderson, K. Arai, M. C. Araya, S. Ast, S. M. Aston, P. Astone, D. Atkinson, P. Aufmuth, C. Aulbert, B. E. Aylott, S. Babak, P. Baker, G. Ballardin, S. Ballmer, Y. Bao, J. C. B. Barayoga, D. Barker, F. Barone, B. Barr, L. Barsotti, M. Barsuglia, M. A. Barton, I. Bartos, R. Bassiri, M. Bastarrika, A. Basti, J. Batch, J. Bauchrowitz, T. S. Bauer, M. Bebronne, D. Beck, B. Behnke, M. Bejger, M. G. Beker, A. S. Bell, C. Bell, I. Belopolski, M. Benacquista, J. M. Berliner, A. Bertolini, J. Betzwieser, N. Beveridge, P. T. Beyersdorf, T. Bhadbade, I. A. Bilenko, G. Billingsley, J. Birch, R. Biswas, M. Bitossi, M. A. Bizouard, E. Black, J. K. Blackburn, L. Blackburn, D. Blair, B. Bland, M. Blom, O. Bock, T. P. Bodiya, C. Bogan, C. Bond, R. Bondarescu, F. Bondu, L. Bonelli, R. Bonnand, R. Bork, M. Born, V. Boschi, S. Bose, L. Bosi, B. Bouhou, S. Braccini, C. Bradaschia, P. R. Brady, V. B. Braginsky, M. Branchesi, J. E. Brau, J. Breyer, T. Briant, D. O. Bridges, A. Brillet, M. Brinkmann, V. Brisson, M. Britzger, A. F. Brooks, D. A. Brown, T. Bulik, H. J. Bulten, A. Buonanno, J. Burguet-Castell, D. Buskulic, C. Buy, R. L. Byer, L. Cadonati, G. Cagnoli, E. Calloni, J. B. Camp, P. Campsie, K. Cannon, B. Canuel, J. Cao, C. D. Capano, F. Carbognani, L. Carbone, S. Caride, S. Caudill, M. Cavaglià, F. Cavalier, R. Cavalieri, G. Cella,

C. Cepeda, E. Cesarini, T. Chalermsongsak, P. Charlton, E. Chassande-Mottin, W. Chen, X. Chen, Y. Chen, A. Chincarini, A. Chiummo, H. S. Cho, J. Chow, N. Christensen, S. S. Y. Chua, C. T. Y. Chung, S. Chung, G. Ciani, F. Clara, D. E. Clark, J. A. Clark, J. H. Clayton, F. Cleva, E. Coccia, P. F. Cohadon, C. N. Colacino, A. Colla, M. Colombini, A. Conte, R. Conte, D. Cook, T. R. Corbitt, M. Cordier, N. Cornish, A. Corsi, C. A. Costa, M. Coughlin, J. P. Coulon, P. Couvares, D. M. Coward, M. Cowart, D. C. Coyne, J. D. E. Creighton, T. D. Creighton, A. M. Cruise, A. Cumming, L. Cunningham, E. Cuoco, R. M. Cutler, K. Dahl, M. Damjanic, S. L. Danilishin, S. D'Antonio, K. Danzmann, V. Dattilo, B. Daudert, H. Daveloza, M. Davier, E. J. Daw, T. Dayanga, R. De Rosa, D. DeBra, G. Debreczeni, J. Degallaix, W. Del Pozzo, T. Dent, V. Dergachev, R. DeRosa, S. Dhurandhar, L. Di Fiore, A. Di Lieto, I. Di Palma, M. Di Paolo Emilio, A. Di Virgilio, M. Díaz, A. Dietz, F. Donovan, K. L. Dooley, S. Doravari, S. Dorsher, M. Drago, R. W. P. Drever, J. C. Driggers, Z. Du, J. C. Dumas, S. Dwyer, T. Eberle, M. Edgar, M. Edwards, A. Effler, P. Ehrens, G. Endrőczi, R. Engel, T. Etzel, K. Evans, M. Evans, T. Evans, M. Factourovich, V. Fafone, S. Fairhurst, B. F. Farr, W. M. Farr, M. Favata, D. Fazi, H. Fehrmann, D. Feldbaum, F. Feroz, I. Ferrante, F. Ferrini, F. Fidecaro, L. S. Finn, I. Fiori, R. P. Fisher, R. Flaminio, S. Foley, E. Forsi, L. A. Forte, N. Fotopoulos, J. D. Fournier, J. Franc, S. Franco, S. Frasca, F. Frasconi, M. Frede, M. A. Frei, Z. Frei, A. Freise, R. Frey, T. T. Fricke, D. Friedrich, P. Fritschel, V. V. Frolov, M. K. Fujimoto, P. J. Fulda, M. Fyffe, J. Gair, M. Galimberti, L. Gammaitoni, J. Garcia, F. Garufi, M. E. Gáspár, G. Gelencser, G. Gemme, E. Genin, A. Gennai, L. Á. Gergely, S. Ghosh, J. A. Giaime, S. Giampanis, K. D. Giardina, A. Giazotto, S. Gil-Casanova, C. Gill, J. Gleason, E. Goetz, G. González, M. L. Gorodetsky, S. Goßler, R. Gouaty, C. Graef, P. B. Graff, M. Granata, A. Grant, C. Gray, R. J. S. Greenhalgh, A. M. Gretarsson, C. Griffo, H. Grote, K. Grover, S. Grunewald, G. M. Guidi, C. Guido, R. Gupta, E. K. Gustafson, R. Gustafson, J. M. Hallam, D. Hammer, G. Hammond, J. Hanks, C. Hanna, J. Hanson, J. Harms, G. M. Harry, I. W. Harry, E. D. Harstad, M. T. Hartman, C. J. Haster, K. Haughian, K. Hayama, J. F. Hayau, J. Heefner, A. Heidmann, M. C. Heintze, H. Heitmann, P. Hello, G. Hemming, M. A. Hendry, I. S. Heng, A. W. Heptonstall, V. Herrera, M. Heurs, M. Hewitson, S. Hild, D. Hoak, K. A. Hodge, K. Holt, M. Holtrop, T. Hong, S. Hooper, J. Hough, E. J. Howell, B. Hughey, S. Husa, S. H. Huttner, T. Huynh-Dinh, D. R. Ingram, R. Inta, T. Isogai, A. Ivanov, K. Izumi, M. Jacobson, E. James, Y. J. Jang, P. Jaranowski, E. Jesse, W. W. Johnson, D. I. Jones, R. Jones, R. J. G. Jonker, L. Ju, P. Kalmus, V. Kalogera, S. Kandhasamy, G. Kang, J. B. Kanner, M. Kasprzack, R. Kasturi, E. Katsavounidis, W. Katzman, H. Kaufer, K. Kaufman, K. Kawabe, S. Kawamura, F. Kawazoe, D. Keitel, D. Kelley, W. Kells, D. G. Keppel, Z. Keresztes, A. Khalaidovski, F. Y. Khalili, E. A. Khazanov, B. K. Kim, C. Kim, H. Kim, K. Kim, N. Kim, Y. M. Kim, P. J. King, D. L. Kinzel, J. S. Kissel, S. Klimenko, J. Kline, K. Kokeyama, V. Kondrashov, S. Koranda, W. Z. Korth, I. Kowalska, D. Kozak, V. Kringel, B. Krishnan, A. Królak, G. Kuehn, P. Kumar, R. Kumar, R. Kurdyumov, P. Kwee, P. K. Lam, M. Land ry, A. Langley, B. Lantz, N. Lastzka, C. Lawrie, A. Lazzarini, A. Le Roux, P. Leaci, C. H. Lee, H. K. Lee, H. M. Lee, J. R. Leong, I. Leonor, N. Leroy, N. Letendre,

V. Lhuillier, J. Li, T. G. F. Li, P. E. Lindquist, V. Litvine, Y. Liu, Z. Liu, N. A. Lockerbie, D. Lodhia, J. Logue, M. Lorenzini, V. Loriette, M. Lormand, G. Losurdo, J. Lough, M. Lubinski, H. Lück, A. P. Lundgren, J. Macarthur, E. Macdonald, B. Machenschalk, M. MacInnis, D. M. Macleod, M. Mageswaran, K. Mailand, E. Majorana, I. Maksimovic, V. Malvezzi, N. Man, I. Mandel, V. Mandic, M. Mantovani, F. Marchesoni, F. Marion, S. Márka, Z. Márka, A. Markosyan, E. Maros, J. Marque, F. Martelli, I. W. Martin, R. M. Martin, J. N. Marx, K. Mason, A. Masserot, F. Matichard, L. Matone, R. A. Matzner, N. Mavalvala, G. Mazzolo, R. McCarthy, D. E. McClelland , S. C. McGuire, G. McIntyre, J. McIver, G. D. Meadors, M. Mehmet, T. Meier, A. Melatos, A. C. Melissinos, G. Mendell, D. F. Menéndez, R. A. Mercer, S. Meshkov, C. Messenger, M. S. Meyer, H. Miao, C. Michel, L. Milano, J. Miller, Y. Minenkov, C. M. F. Mingarelli, V. P. Mitrofanov, G. Mitselmakher, R. Mittleman, B. Moe, M. Mohan, S. R. P. Mohapatra, D. Moraru, G. Moreno, N. Morgado, A. Morgia, T. Mori, S. R. Morriss, S. Mosca, K. Mossavi, B. Mours, C. M. Mow-Lowry, C. L. Mueller, G. Mueller, S. Mukherjee, A. Mullavey, H. Müller-Ebhardt, J. Munch, D. Murphy, P. G. Murray, A. Mytidis, T. Nash, L. Naticchioni, V. Necula, J. Nelson, I. Neri, G. Newton, T. Nguyen, A. Nishizawa, A. Nitz, F. Nocera, D. Nolting, M. E. Normandin, L. Nuttall, E. Ochsner, J. O'Dell, E. Oelker, G. H. Ogin, J. J. Oh, S. H. Oh, R. G. Oldenberg, B. O'Reilly, R. O'Shaughnessy, C. Osthelder, C. D. Ott, D. J. Ottaway, R. S. Ottens, H. Overmier, B. J. Owen, A. Page, L. Palladino, C. Palomba, Y. Pan, C. Pankow, F. Paoletti, R. Paoletti, M. A. Papa, M. Parisi, A. Pasqualetti, R. Passaquieti, D. Passuello, M. Pedraza, S. Penn, A. Perreca, G. Persichetti, M. Phelps, M. Pichot, M. Pickenpack, F. Piergiovanni, V. Pierro, M. Pihlaja, L. Pinard, I. M. Pinto, M. Pitkin, H. J. Pletsch, M. V. Plissi, R. Poggiani, J. Pöld, F. Postiglione, C. Poux, M. Prato, V. Predoi, T. Prestegard, L. R. Price, M. Prijatelj, M. Principe, S. Privitera, G. A. Prodi, L. G. Prokhorov, O. Puncken, M. Punturo, P. Puppo, V. Quetschke, R. Quitzow-James, F. J. Raab, D. S. Rabeling, I. Rácz, H. Radkins, P. Raffai, M. Rakhmanov, C. Ramet, B. Rankins, P. Rapagnani, V. Raymond, V. Re, C. M. Reed, T. Reed, T. Regimbau, S. Reid, D. H. Reitze, F. Ricci, R. Riesen, K. Riles, M. Roberts, N. A. Robertson, F. Robinet, C. Robinson, E. L. Robinson, A. Rocchi, S. Roddy, C. Rodriguez, M. Rodruck, L. Rolland, J. G. Rollins, R. Romano, J. H. Romie, D. Rosińska, C. Röver, S. Rowan, A. Rüdiger, P. Ruggi, K. Ryan, F. Salemi, L. Sammut, V. Sandberg, S. Sankar, V. Sannibale, L. Santamaría, I. Santiago-Prieto, G. Santostasi, E. Saracco, B. Sassolas, B. S. Sathyaprakash, P. R. Saulson, R. L. Savage, R. Schilling, R. Schnabel, R. M. S. Schofield, B. Schulz, B. F. Schutz, P. Schwinberg, J. Scott, S. M. Scott, F. Seifert, D. Sellers, D. Sentenac, A. Sergeev, D. A. Shaddock, M. Shaltev, B. Shapiro, P. Shawhan, D. H. Shoemaker, T. L. Sidery, X. Siemens, D. Sigg, D. Simakov, A. Singer, L. Singer, A. M. Sintes, G. R. Skelton, B. J. J. Slagmolen, J. Slutsky, J. R. Smith, M. R. Smith, R. J. E. Smith, N. D. Smith-Lefebvre, K. Somiya, B. Sorazu, F. C. Speirits, L. Sperand io, M. Stefszky, E. Steinert, J. Steinlechner, S. Steinlechner, S. Steplewski, A. Stochino, R. Stone, K. A. Strain, S. E. Strigin, A. S. Stroeer, R. Sturani, A. L. Stuver, T. Z. Summerscales, M. Sung, S. Susmithan, P. J. Sutton, B. Swinkels, G. Szeifert, M. Tacca, L. Taffarello, D. Talukder, D. B. Tanner, S. P. Tarabrin, R. Taylor,

A. P. M. ter Braack, P. Thomas, K. A. Thorne, K. S. Thorne, E. Thrane, A. Thüring, C. Titsler, K. V. Tokmakov, C. Tomlinson, A. Toncelli, M. Tonelli, O. Torre, C. V. Torres, C. I. Torrie, E. Tournefier, F. Travasso, G. Traylor, M. Tse, D. Ugolini, H. Vahlbruch, G. Vajente, J. F. J. van den Brand, C. Van Den Broeck, S. van der Putten, A. A. van Veggel, S. Vass, M. Vasuth, R. Vaulin, M. Vavoulidis, A. Vecchio, G. Vedovato, J. Veitch, P. J. Veitch, K. Venkateswara, D. Verkindt, F. Vetrano, A. Viceré, A. E. Villar, J. Y. Vinet, S. Vitale, H. Vocca, C. Vorvick, S. P. Vyatchanin, A. Wade, L. Wade, M. Wade, S. J. Waldman, L. Wallace, Y. Wan, M. Wang, X. Wang, A. Wanner, R. L. Ward, M. Was, M. Weinert, A. J. Weinstein, R. Weiss, T. Welborn, L. Wen, P. Wessels, M. West, T. Westphal, K. Wette, J. T. Whelan, S. E. Whitcomb, D. J. White, B. F. Whiting, K. Wiesner, C. Wilkinson, P. A. Willems, L. Williams, R. Williams, B. Willke, M. Wimmer, L. Winkelmann, W. Winkler, C. C. Wipf, A. G. Wiseman, H. Wittel, G. Woan, R. Wooley, J. Worden, J. Yablon, I. Yakushin, H. Yamamoto, K. Yamamoto, C. C. Yancey, H. Yang, D. Yeaton-Massey, S. Yoshida, M. Yvert, A. Zadrożny, M. Zanolin, J. P. Zendri, F. Zhang, L. Zhang, C. Zhao, N. Zotov, M. E. Zucker, and J. Zweizig. Parameter estimation for compact binary coalescence signals with the first generation gravitational-wave detector network. , 88:062001, Sep 2013.

[12] B. P. Abbott, R. Abbott, T. D. Abbott, M. R. Abernathy, F. Acernese, K. Ackley, C. Adams, T. Adams, P. Addesso, R. X. Adhikari, V. B. Adya, C. Affeldt, M. Agathos, K. Agatsuma, N. Aggarwal, O. D. Aguiar, L. Aiello, A. Ain, P. Ajith, T. Akutsu, B. Allen, A. Allocca, P. A. Altin, A. Ananyeva, S. B. Anderson, W. G. Anderson, M. Ando, S. Appert, K. Arai, A. Araya, M. C. Araya, J. S. Areeda, N. Arnaud, K. G. Arun, H. Asada, S. Ascenzi, G. Ashton, Y. Aso, M. Ast, S. M. Aston, P. Astone, S. Atsuta, P. Aufmuth, C. Aulbert, A. Avila-Alvarez, K. Awai, S. Babak, P. Bacon, M. K. M. Bader, L. Baiotti, P. T. Baker, F. Baldaccini, G. Ballardin, S. W. Ballmer, J. C. Barayoga, S. E. Barclay, B. C. Barish, D. Barker, F. Barone, B. Barr, L. Barsotti, M. Barsuglia, D. Barta, J. Bartlett, M. A. Barton, I. Bartos, R. Bassiri, A. Basti, J. C. Batch, C. Baune, V. Bavigadda, M. Bazzan, B. Bécsy, C. Beer, M. Bejger, I. Belahcene, M. Belgin, A. S. Bell, B. K. Berger, G. Bergmann, C. P. L. Berry, D. Bersanetti, A. Bertolini, J. Betzwieser, S. Bhagwat, R. Bhandare, I. A. Bilenko, G. Billingsley, C. R. Billman, J. Birch, R. Birney, O. Birnholtz, S. Biscans, A. Bisht, M. Bitossi, C. Biwer, M. A. Bizouard, J. K. Blackburn, J. Blackman, C. D. Blair, D. G. Blair, R. M. Blair, S. Bloemen, O. Bock, M. Boer, G. Bogaert, A. Bohe, F. Bondu, R. Bonnand, B. A. Boom, R. Bork, V. Boschi, S. Bose, Y. Bouffanais, A. Bozzi, C. Bradaschia, P. R. Brady, V. B. Braginsky, M. Branchesi, J. E. Brau, T. Briant, A. Brillet, M. Brinkmann, V. Brisson, P. Brockill, J. E. Broida, A. F. Brooks, D. A. Brown, D. D. Brown, N. M. Brown, S. Brunett, C. C. Buchanan, A. Buikema, T. Bulik, H. J. Bulten, A. Buonanno, D. Buskulic, C. Buy, R. L. Byer, M. Cabero, L. Cadonati, G. Cagnoli, C. Cahillane, J. Calderón Bustillo, T. A. Callister, E. Calloni, J. B. Camp, K. C. Cannon, H. Cao, J. Cao, C. D. Capano, E. Capocasa, F. Carbognani, S. Caride, J. Casanueva Diaz, C. Casentini, S. Caudill, M. Cavaglià, F. Cavalier, R. Cavalieri, G. Cella, C. B. Cepeda, L. Cerboni Baiardi, G. Cerretani, E. Cesarini, S. J. Chamberlin, M. Chan,

S. Chao, P. Charlton, E. Chassande-Mottin, B. D. Cheeseboro, H. Y. Chen, Y. Chen, H.-P. Cheng, A. Chincarini, A. Chiummo, T. Chmiel, H. S. Cho, M. Cho, J. H. Chow, N. Christensen, Q. Chu, A. J. K. Chua, S. Chua, S. Chung, G. Ciani, F. Clara, J. A. Clark, F. Cleva, C. Cocchieri, E. Coccia, P.-F. Cohadon, A. Colla, C. G. Collette, L. Cominsky, M. Constancio, L. Conti, S. J. Cooper, T. R. Corbitt, N. Cornish, A. Corsi, S. Cortese, C. A. Costa, M. W. Coughlin, S. B. Coughlin, J.-P. Coulon, S. T. Countryman, P. Couvares, P. B. Covas, E. E. Cowan, D. M. Coward, M. J. Cowart, D. C. Coyne, R. Coyne, J. D. E. Creighton, T. D. Creighton, J. Cripe, S. G. Crowder, T. J. Cullen, A. Cumming, L. Cunningham, E. Cuoco, T. D. Canton, S. L. Danilishin, S. D'Antonio, K. Danzmann, A. Dasgupta, C. F. Da Silva Costa, V. Dattilo, I. Dave, M. Davier, G. S. Davies, D. Davis, E. J. Daw, B. Day, R. Day, S. De, D. DeBra, G. Debreczeni, J. Degallaix, M. De Laurentis, S. Deléglise, W. Del Pozzo, T. Denker, T. Dent, V. Dergachev, R. De Rosa, R. T. DeRosa, R. DeSalvo, R. C. Devine, S. Dhurandhar, M. C. Díaz, L. D. Fiore, M. D. Giovanni, T. D. Girolamo, A. D. Lieto, S. D. Pace, I. D. Palma, A. D. Virgilio, Z. Doctor, K. Doi, V. Dolique, F. Donovan, K. L. Dooley, S. Doravari, I. Dorrington, R. Douglas, M. Dovale Álvarez, T. P. Downes, M. Drago, R. W. P. Drever, J. C. Driggers, Z. Du, M. Ducrot, S. E. Dwyer, K. Eda, T. B. Edo, M. C. Edwards, A. Effler, H.-B. Eggenstein, P. Ehrens, J. Eichholz, S. S. Eikenberry, R. A. Eisenstein, R. C. Essick, Z. Etienne, T. Etzel, M. Evans, T. M. Evans, R. Everett, M. Factourovich, V. Fafone, H. Fair, S. Fairhurst, X. Fan, S. Farinon, B. Farr, W. M. Farr, E. J. Fauchon-Jones, and M. Favata. Prospects for observing and localizing gravitational-wave transients with advanced ligo, advanced virgo and kagra. *Living Reviews in Relativity*, 21(1):3, Apr 2018.

[13] B. P. Abbott, The LIGO Scientific Collaboration, Virgo Collaboration, et al. Prospects for observing and localizing gravitational-wave transients with advanced ligo and advanced virgo. *Living Reviews in Relativity*, 19(1):1, Feb 2016.

[14] T. Accadia et al. Virgo: a laser interferometer to detect gravitational waves. *JINST*, 7:P03012, 2012.

[15] M. Alcubierre. Introduction to 3+1 numerical relativity. *Introduction to 3+1 Numerical Relativity*, 04 2006.

[16] M. Alcubierre, B. Brügmann, P. Diener, M. Koppitz, D. Pollney, E. Seidel, and R. Takahashi. Gauge conditions for long-term numerical black hole evolutions without excision. , 67:084023, Apr 2003.

[17] M. Alcubierre, B. Brügmann, T. Dramlitsch, J. A. Font, P. Papadopoulos, E. Seidel, N. Stergioulas, and R. Takahashi. Towards a stable numerical evolution of strongly gravitating systems in general relativity: The conformal treatments. , 62:044034, Aug 2000.

[18] D. Alic, L. Rezzolla, I. Hinder, and P. Mösta. Dynamical damping terms for symmetry-seeking shift conditions. *Classical and Quantum Gravity*, 27:245023, Dec 2010.

[19] P. Amaro-Seoane, H. Audley, S. Babak, J. Baker, E. Barausse, P. Bender, E. Berti, P. Binetruy, M. Born, D. Bortoluzzi, J. Camp, C. Caprini, V. Cardoso, M. Colpi, J. Conklin,

N. Cornish, C. Cutler, K. Danzmann, R. Dolesi, L. Ferraioli, V. Ferroni, E. Fitzsimons, J. Gair, L. Gesa Bote, D. Giardini, F. Gibert, C. Grimani, H. Halloin, G. Heinzel, T. Hertog, M. Hewitson, K. Holley-Bockelmann, D. Hollington, M. Hueller, H. Inchauspe, P. Jetzer, N. Karnesis, C. Killow, A. Klein, B. Klipstein, N. Korsakova, S. L. Larson, J. Livas, I. Lloro, N. Man, D. Mance, J. Martino, I. Mateos, K. McKenzie, S. T. McWilliams, C. Miller, G. Mueller, G. Nardini, G. Nelemans, M. Nofrarias, A. Petiteau, P. Pivato, E. Plagnol, E. Porter, J. Reiche, D. Robertson, N. Robertson, E. Rossi, G. Russano, B. Schutz, A. Sesana, D. Shoemaker, J. Slutsky, C. F. Sopuerta, T. Sumner, N. Tamanini, I. Thorpe, M. Troebs, M. Vallisneri, A. Vecchio, D. Vetrugno, S. Vitale, M. Volonteri, G. Wanner, H. Ward, P. Wass, W. Weber, J. Ziemer, and P. Zweifel. Laser Interferometer Space Antenna. *arXiv e-prints*, page arXiv:1702.00786, Feb 2017.

[20] P. Anninos. Plane-symmetric cosmology with relativistic hydrodynamics. *Phys. Rev. D*, 58:064010, Aug 1998.

[21] M. Ansorg, B. Brügmann, and W. Tichy. Single-domain spectral method for black hole puncture data. , 70:064011, Sep 2004.

[22] R. Arnowitt, S. Deser, and C. W. Misner. Republication of: The dynamics of general relativity. *General Relativity and Gravitation*, 40:1997–2027, Sep 2008.

[23] R. Bartnik and J. Isenberg. The constraint equations. In P. T. Chruściel and H. Friedrich, editors, *The Einstein Equations and the Large Scale Behavior of Gravitational Fields*, pages 1–38, Basel, 2004. Birkhäuser Basel.

[24] T. W. Baumgarte and S. L. Shapiro. Numerical integration of einstein's field equations. *Phys. Rev. D*, 59:024007, Dec 1998.

[25] T. W. Baumgarte and S. L. Shapiro. Numerical relativity and compact binaries. , 376:41–131, Mar 2003.

[26] E. Bentivegna. Automatically generated code for relativistic inhomogeneous cosmologies. , 95:044046, Feb 2017.

[27] C. Bona, J. Massó, E. Seidel, and J. Stela. New Formalism for Numerical Relativity. , 75:600–603, Jul 1995.

[28] M. Campanelli, C. O. Lousto, P. Marronetti, and Y. Zlochower. Accurate Evolutions of Orbiting Black-Hole Binaries without Excision. , 96:111101, Mar 2006.

[29] M. Campanelli, C. O. Lousto, P. Marronetti, and Y. Zlochower. Accurate Evolutions of Orbiting Black-Hole Binaries without Excision. , 96:111101, Mar 2006.

[30] Y. Choquet-Bruhat. New elliptic system and global solutions for the constraints equations in general relativity. *Communications in Mathematical Physics*, 21(3):211–218, Sep 1971.

[31] P. Colella and P. R. Woodward. The piecewise parabolic method (ppm) for gas-dynamical simulations. *Journal of Computational Physics*, 54(1):174 – 201, 1984.

[32] G. F. R. Ellis, R. Maartens, and M. A. H. MacCallum. *Relativistic Cosmology*. Cambridge University Press, 2012.

[33] Z. B. Etienne, V. Paschalidis, R. Haas, P. Mösta, and S. L. Shapiro. IllinoisGRMHD: an open-source, user-friendly GRMHD code for dynamical spacetimes. *Classical and Quantum Gravity*, 32:175009, Sep 2015.

[34] J. A. Font. Numerical hydrodynamics and magnetohydrodynamics in general relativity. *Living Reviews in Relativity*, 11(1):7, Sep 2008.

[35] Y. FOURÈS-BRUHAT. Sur l'intégration des Équations de la relativité générale. *Journal of Rational Mechanics and Analysis*, 5(6):951–966, 1956.

[36] R. B. G. Montani, M. Battisti. Primordial Cosmology. *World Scientific*, 2010.

[37] G. González. Gravitational Wave Detectors:. a Report from Ligo-Land. In *Recent Developments in Gravity*, pages 26–33, Jan 2003.

[38] T. Goodale, G. Allen, G. Lanfermann, J. Massó, T. Radke, E. Seidel, and J. Shalf. The Cactus framework and toolkit: Design and applications. In *Vector and Parallel Processing – VECPAR'2002, 5th International Conference, Lecture Notes in Computer Science*, Berlin, 2003. Springer.

[39] E. Gourgoulhon. 3+1 Formalism and Bases of Numerical Relativity. *arXiv e-prints*, pages gr–qc/0703035, Mar. 2007.

[40] J. Healy, C. O. Lousto, I. Ruchlin, and Y. Zlochower. Evolutions of unequal mass, highly spinning black hole binaries. , 97:104026, May 2018.

[41] J. Healy, C. O. Lousto, Y. Zlochower, and M. Campanelli. The RIT binary black hole simulations catalog. *Classical and Quantum Gravity*, 34:224001, Nov. 2017.

[42] S. Husa, I. Hinder, and C. Lechner. Kranc: a Mathematica package to generate numerical codes for tensorial evolution equations. *Computer Physics Communications*, 174:983–1004, June 2006.

[43] J. Ibáñez and J. Martı. Riemann solvers in relativistic astrophysics. *Journal of Computational and Applied Mathematics*, 109(1):173 – 211, 1999.

[44] K. Jani, J. Healy, J. A. Clark, L. London, P. Laguna, and D. Shoemaker. Georgia tech catalog of gravitational waveforms. *Classical and Quantum Gravity*, 33:204001, Oct. 2016.

[45] H.-O. Kreiss and J. Lorenz. Stability for time-dependent differential equations. *Acta Numerica*, 7:203 – 285, 01 1998.

[46] L. Lehner. TOPICAL REVIEW: Numerical relativity: a review. *Classical and Quantum Gravity*, 18:R25–R86, Sep 2001.

[47] A. Lichnerowicz. L'intégration des équations de la gravitation relativiste et le problème des n corps. *J. Math. Pures Appl*, 23, 1944.

[48] A. Lichnérowicz. Sur les équations relativistes de la gravitation. *Bulletin de la Société Mathématique de France*, 80:237–251, 1952.

[49] Ligo Scientific Collaboration et al. A gravitational wave observatory operating beyond the quantum shot-noise limit. *Nature Physics*, 7:962–965, Dec 2011.

[50] F. Löffler, J. Faber, E. Bentivegna, T. Bode, P. Diener, R. Haas, I. Hinder, B. C. Mundim, C. D. Ott, E. Schnetter, G. Allen, M. Campanelli, and P. Laguna. The Einstein Toolkit: a community computational infrastructure for relativistic astrophysics. *Classical and Quantum Gravity*, 29:115001, Jun 2012.

[51] A. M Sintes, P. Aufmuth, C. Aulbert, S. Babak, R. Balasubramanian, B. W Barr, S. Berukoff, S. Borger, C. Gianpietro, C. A. Cantley, M. Casey, S. Chelkowski, D. Churches, C. N. Colacino, D. R. M. Crooks, C. Cutler, K. Danzmann, R. Davies, R. Dupuis, and I. Zawischa. Detector characterization in geo 600. *Classical and Quantum Gravity*, 20, 09 2003.

[52] E. Macaulay, R. C. Nichol, D. Bacon, D. Brout, T. M. Davis, B. Zhang, B. A. Bassett, D. Scolnic, A. Möller, C. B. D'Andrea, S. R. Hinton, R. Kessler, A. G. Kim, J. Lasker, C. Lidman, M. Sako, M. Smith, M. Sullivan, T. M. C. Abbott, S. Allam, J. Annis, J. Asorey, S. Avila, K. Bechtol, D. Brooks, P. Brown, D. L. Burke, J. Calcino, A. Carnero Rosell, D. Carollo, M. Carrasco Kind, J. Carretero, F. J. Castander, T. Collett, M. Crocce, C. E. Cunha, L. N. da Costa, C. Davis, J. De Vicente, H. T. Diehl, P. Doel, A. Drlica-Wagner, T. F. Eifler, J. Estrada, A. E. Evrard, D. A. Finley, B. Flaugher, R. J. Foley, P. Fosalba, J. Frieman, L. Galbany, J. García-Bellido, E. Gaztanaga, K. Glazebrook, S. González-Gaitán, D. Gruen, R. A. Gruendl, J. Gschwend, G. Gutierrez, W. G. Hartley, D. L. Hollowood, K. Honscheid, J. K. Hoormann, B. Hoyle, D. Huterer, B. Jain, D. J. James, T. Jeltema, E. Kasai, E. Krause, K. Kuehn, N. Kuropatkin, O. Lahav, G. F. Lewis, T. S. Li, M. Lima, H. Lin, M. A. G. Maia, J. L. Marshall, P. Martini, R. Miquel, P. Nugent, A. Palmese, Y. C. Pan, A. A. Plazas, A. K. Romer, A. Roodman, E. Sanchez, V. Scarpine, R. Schindler, M. Schubnell, S. Serrano, I. Sevilla-Noarbe, R. Sharp, M. Soares-Santos, F. Sobreira, N. E. Sommer, E. Suchyta, E. Swann, M. E. C. Swanson, G. Tarle, D. Thomas, R. C. Thomas, B. E. Tucker, S. A. Uddin, V. Vikram, A. R. Walker, and P. Wiseman. First Cosmological Results using Type Ia Supernovae from the Dark Energy Survey: Measurement of the Hubble Constant. *arXiv e-prints*, page arXiv:1811.02376, Nov 2018.

[53] P. Marronetti, W. Tichy, B. Brügmann, J. González, M. Hannam, S. Husa, and U. Sperhake. Binary black holes on a budget: simulations using workstations. *Classical and Quantum Gravity*, 24:S43–S58, Jun 2007.

[54] C. W. Misner, K. S. Thorne, and J. A. Wheeler. *Gravitation*. Physics Series. W. H. Freeman, San Francisco, first edition edition, Sept. 1973.

[55] P. Mösta, B. C. Mundim, J. A. Faber, R. Haas, S. C. Noble, T. Bode, F. Löffler, C. D. Ott, C. Reisswig, and E. Schnetter. GRHydro: a new open-source general-relativistic magneto-hydrodynamics code for the Einstein toolkit. *Classical and Quantum Gravity*, 31:015005, Jan 2014.

[56] A. H. Mroué, M. A. Scheel, B. Szilágyi, H. P. Pfeiffer, M. Boyle, D. A. Hemberger, L. E. Kidder, G. Lovelace, S. Ossokine, N. W. Taylor, A. Zenginoğlu, L. T. Buchman, T. Chu, E. Foley, M. Giesler, R. Owen, and S. A. Teukolsky. Catalog of 174 Binary Black Hole Simulations for Gravitational Wave Astronomy. , 111:241104, Dec. 2013.

[57] D. Müller, J. Grigsby, and B. Brügmann. Dynamical shift condition for unequal mass black hole binaries. , 82:064004, Sep 2010.

[58] S. Noble, C. Gammie, J. Mckinney, and L. Del Zanna. Primitive variable solvers for conservative general relativistic magnetohydrodynamics. *Astrophysical Journal*, 641(1 I):626–637, 4 2006.

[59] N. O Murchadha and J. J. York. Initial-value problem of general relativity. i. general formulation and physical interpretation. *Phys. Rev., D., v. 10, no. 2, pp. 428-436.*

[60] A. L. P. Hobson, G. Efstathiou. General Relativity: An Introduction for Physicists. *Cambridge University Press*, 2006.

[61] H. P. Pfeiffer. The initial value problem in numerical relativity. *arXiv e-prints*, pages gr–qc/0412002, Dec 2004.

[62] H. P. Pfeiffer and J. W. York. Extrinsic curvature and the Einstein constraints. , 67:044022, Feb 2003.

[63] W. Rindler. Relativity: Special, General, and Cosmological. *Oxford University Press*, 2001.

[64] G. E. S. Hawking. The Large Scale Structure of Space-Time. *Cambridge Mono-graphs on Mathematical Physics.*, 1973.

[65] O. Sarbach, G. Calabrese, J. Pullin, and M. Tiglio. Hyperbolicity of the Baumgarte-Shapiro-Shibata-Nakamura system of Einstein evolution equations. , 66:064002, Sep 2002.

[66] E. Schnetter, S. H. Hawley, and I. Hawke. Evolutions in 3D numerical relativity using fixed mesh refinement. *Classical and Quantum Gravity*, 21:1465–1488, Mar 2004.

[67] M. Shibata and T. Nakamura. Evolution of three-dimensional gravitational waves: Harmonic slicing case. *Phys. Rev. D*, 52:5428–5444, Nov 1995.

[68] L. Smarr and J. W. York. Kinematical conditions in the construction of spacetime. *Phys. Rev. D*, 17:2529–2551, May 1978.

[69] L. Smarr and J. W. York. Radiation gauge in general relativity. *Phys. Rev. D*, 17:1945–1956, Apr 1978.

[70] The LIGO Scientific Collaboration, the Virgo Collaboration, et al. GWTC-1: A Gravitational-Wave Transient Catalog of Compact Binary Mergers Observed by LIGO and Virgo during the First and Second Observing Runs. *arXiv e-prints*, page arXiv:1811.12907, Nov 2018.

[71] J. Thornburg. A 3+1 Computational Scheme for Dynamic Spherically Symmetric Black Hole Spacetimes – II: Time Evolution. *arXiv e-prints*, pages gr–qc/9906022, Jun 1999.

[72] J. R. van Meter, J. G. Baker, M. Koppitz, and D.-I. Choi. How to move a black hole without excision: Gauge conditions for the numerical evolution of a moving puncture. , 73:124011, Jun 2006.

[73] T. W.Baumgarte and S. L.Shapiro. Numerical relativity and compact binaries. *Physics Report*, 376(2):41–131, 2003.

[74] B. Wendroff. *Approximate Riemann Solvers, Godunov Schemes and Contact Discontinuities*, pages 1023–1056. Springer US, Boston, MA, 2001.

[75] J. R. Wilson. Numerical Study of Fluid Flow in a Kerr Space. , 173:431, Apr. 1972.

[76] J. R. Wilson and G. J. Mathews. *Relativistic Numerical Hydrodynamics*. Cambridge Monographs on Mathematical Physics. Cambridge University Press, 2003.

[77] J. W. York. Gravitational degrees of freedom and the initial-value problem. *Phys. Rev. Lett.*, 26:1656–1658, Jun 1971.

[78] J. W. York. Mapping onto solutions of the gravitational initial value problem. *Journal of Mathematical Physics*, 13(2):125–130, 1972.

[79] J. W. York. Role of conformal three-geometry in the dynamics of gravitation. *Phys. Rev. Lett.*, 28:1082–1085, Apr 1972.

[80] J. W. York. Conformally invariant orthogonal decomposition of symmetric tensors on riemannian manifolds and the initial-value problem of general relativity. *Journal of Mathematical Physics*, 14(4):456–464, 1973.

[81] J. W. York. Conformal "thin-sandwich" data for the initial-value problem of general relativity. *Phys. Rev. Lett.*, 82:1350–1353, Feb 1999.

[82] J. W. York, Jr. Kinematics and dynamics of general relativity. In L. L. Smarr, editor, *Sources of Gravitational Radiation*, pages 83–126, 1979.

[83] J. W. York, Jr. Kinematics and dynamics of general relativity. In L. L. Smarr, editor, *Sources of Gravitational Radiation*, pages 83–126, 1979.

[84] M. Zilhão and F. Löffler. An Introduction to the Einstein Toolkit. *International Journal of Modern Physics A*, 28:1340014–126, Sep 2013.